PhD Course in Biochemistry
BEMM Doctorate School
Department of Biochemical Sciences "A. Rossi Fanelli"
XXXIV Cycle (2018-2021)

"Engineered Human Nanoferritin For Cancer Therapy: Development and Biophysical characterization"

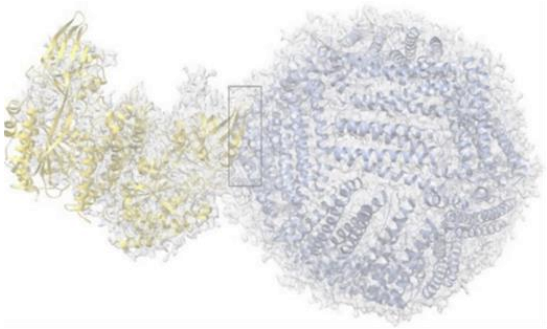

PhD candidate :
Dr. Martina Pitea

Supervisor:
Prof. Alberto Boffi

Tutor:
Dr. Pierpaolo Ceci

Coordinator:
Prof. Stefano Gianni

13th December 2021

Acknowledgements

This PhD Thesis was mainly performed at the Department of Biochemical Sciences "A. Rossi Fanelli", University of Rome "Sapienza". Firstly, I truly and deeply thank my advisor, Prof. Alberto Boffi for always believing in me and in everything I did during these three years. His enthusiasm for research was an example for me, increasing and growing in me the curiosity and desire for this area.

I thank Dr. Pierpaolo Ceci and Dr. Elisabetta Falvo for their rigorous scientific advice and for their precious academic guidance, for giving me the opportunity to become part of their team and for giving me access to the laboratory and research facilities.

My strong gratitude goes also to the coordinators of the Ph.D. Program in Biochemistry, Prof. Francesco Malatesta and Prof. Stefano Gianni for their supportive and continuous interest in me and in my results during these three years.

A precious help to our project derives from the important external collaborations with the groups of Dr. Giulio Fracasso (University of Verona), Dr. Gianluca Sala (University of Chieti) my acknowledgments are also for the people belonging to their groups. The experimental work of this thesis also arises from a close collaboration with Prof. Alessandro Arcovito from Università Cattolica del Sacro Cuore in Rome, who I wish to thank for his valuable contribution.

Special thanks are also addressed to Dr. Linda Celeste Montemiglio from CNR-IBPM, and Prof. Vallone's group, for involving me in such an interesting project regarding cryo-EM.

My sincere thanks also go to Prof. Carlotta Zamparelli, who has always encouraged and motivated me with great enthusiasm. I learned from her that any difficulty you may encounter in life is easier to deal with a friend by your side.

I wish to thank professors, researchers and students, all the people of the of Biochemical Sciences "A. Rossi Fanelli", who contributed to my personal and scientific growth. I am particularly grateful to CNR-IBPM members, and all the people of XXXIV of Biochemistry Doctorate cycle for their helpful encouragement and friendship.

Last but not least, thanks to my dear mother, my family and my friends for their love and continuous support spiritually throughout writing this thesis and my life in general.

This thesis is dedicated to those who, like me, do not give up in the face of difficulties but find the strength to go forward with a smile and determination.

INDEX

1. INTRODUCTION

Cancer is one of the most dreaded diseases of the 20th century and spreading further with continuance and increasing incidence in the 21st century (Roy and Saikia 2016). The most commonly diagnosed cancers worldwide were those of the lung (1.8 million, 13.0% of the total), breast (1.7 million, 11.9%), and colorectum (1.4 million, 9.7%). Cancer is a group of diseases characterized by the uncontrolled growth and increase of abnormal cells. If the increase is not controlled, it can result in death. Over the past several decades, remarkable breakthroughs have been made in advancing our understanding of how cancer originates and develops, which has in turn lead to better methods for both diagnosis and treatment (Steichen et al., 2013). Although the overall mortality of cancer is showing a declining trend for the first time in five decades, it still remains at a high rate of 20.2% (http://www.iarc.fr/). In all cases, the effectiveness of the treatment is directly related to the treatment's ability to target and to kill the cancer cells while affecting as few healthy cells as possible. The ability of chemotherapy to kill cancer cells depends on its ability to arrest cell division. Usually, cancer drugs work by damaging the Ribonucleic acid (RNA) or Deoxyribonucleic acid (DNA) that tells the cell how to copy itself in division. If the cancer cells are unable to divide, they die. The faster that cancer cells divide, the more likely it is that chemotherapy will kill the cells, causing the tumor to reduce in size. They also induce cell suicide (self-death or apoptosis) (Brown and Attardi 2005; Okada and Mak 2004). Unfortunately, chemotherapy does not know the difference between cancer cells and healthy cells. For this reason, the key challenge in the development of novel therapeutics is to bring the drug to the target tissue

and avoid the biological barriers. In fact, one injected, the carrier/vehicle must pass several impermeable barriers before reaching its final destination such as endothelial and epithelial barriers, enzymatic degradation, mononuclear phagocyte system (MPS), opsonization, interstitial transport, cell membrane, nuclear membrane (Perez and Fernandez Medarde 2015; Sun et al., 2014). Therefore, it would be desirable to develop highly efficient therapeutics, the so-called "magic bullets", that can overcome biological barriers, distinguish between malignant and benign cells, selectively target the cancerous tissues, and "intelligently" respond to the heterogeneous and complex microenvironment inside a tumor for on-demand release of therapeutic agents in the optimal dosage range (Peer et al., 2007; Kreuter 2007). These novel targeted therapies, of increasing interest as evidenced by FDA-approved targeted cancer drugs in recent years, block biologic transduction pathways and/or specific cancer proteins to induce the death of cancer cells by means of apoptosis and stimulation of the immune system, or specifically deliver chemotherapeutic agents to cancer cells, minimizing the undesirable side effects (Pérez-Herrero and Fernández-Medarde 2015). Nanotechnology is the science of engineering materials and systems on a molecular scale. Its application to medicine, nanomedicine, has enabled the development of nanoparticle (NPs) drug-delivery vehicles moving toward the declared goals. One of the main applications for the NP drug carriers has been the delivery of cancer drugs. In this context, tumor targeting of nanomedicines has emerged as a promising approach to overcome the lack of specificity of conventional chemotherapeutic agents (Jain et al., 2010; Martinez et al., 2013). In fact, the use of nanovectors as carriers for therapeutic agents has the potential ability to avoid the biological barriers encountered between the point of

administration and the final target and accumulate at the site of disease. Targeted delivery of anti-cancer therapeutics to cancer cells ("site-specific drug delivery") aims at enhancing accumulation of the drugs within the tumor while guiding them away from potentially healthy tissues (Sun et al., 2014, Pérez-Herrero and Fernández-Medarde 2015).

1.1 Tumor environment and targeting strategies

Understanding the tumor microenvironment and the tumor cell helps out to make clear the problems of drug delivery in cancer. Once a malignant tumor grows to > 2-3 mm^3 in size, the delivery of oxygen and nutrients becomes diffusion limited and the formation of new blood vessels becomes essential to meet the ever increasing demands of the rapidly growing malignant cells (Jones and Harris 1998; Baban and Seymour. 1998). This is accomplished through the release of angiogenic factors by the neoplastic tissue aiming to increase the microvasculature within the tumor in order to carry on further growth (LaRocque et al., 2009). Specific matrix metalloproteinases (MMPs) are engaged in the degradation of extracellular matrices and are tightly associated with malignant processes of tumors, including metastasis and angiogenesis (Overall and Kleifeld, 2006; Corry et al., 2004). The resultant imbalance of angiogenic factors and MMPs within neoplastic tissues results in highly disorganized vessels, which are dilated, with numerous pores and wide gap junctions between endothelial cells (Cho et al., 2008). In contrast to normal tissues, the vasculature of tumors is marked by a heterogeneous distribution of vessel sizes and shapes, generally larger vessel diameters, higher vascular density, and enhanced permeability. The size of the gaps between the leaky

endothelial cells ranges from 100 to 780 nm depending on the tumor type (Hobbs et al., 1998; Rubin and Casarett 1966; Shubik 1982). This contrasts with the tight endothelial junctions of normal vessels typically of 5 to 10 nm size. The tumor interstitium is composed of an elastic network of collagen fibers filled with hydrophilic fluid which has high interstitial pressures offering resistance to the internal flux of molecules (Jain 1987; Heldin et al., 2004). Transport of drugs into the interstitium is determined by the balanced force between the external interstitial pressure and the properties of the diffusing drug including particle size and configuration, hydrophobic nature and electrical charge. Tumor interstitial pressures are higher in the tumor center and lower in the periphery, favoring decreased drug diffusion to the center of tumors (Jain 2001; Jang et al., 2003). Additionally, the lymphatic system inside a tumor is largely absent or dysfunctional with insufficient drainage. Hence, drugs that gain interstitial access may have extended retention times in the tumor interstitium. This phenomenon of leaky vasculature and impaired lymphatic drainage has been referred to as the Enhanced Permeability and Retention effect (EPR) (Maeda et al., 2000, Maeda 2001; Vannucci et al., 2014). In general, nanomedicine-based materials can be delivered to tumors by two strategies: passive and/or active targeting (**Figure 1**).

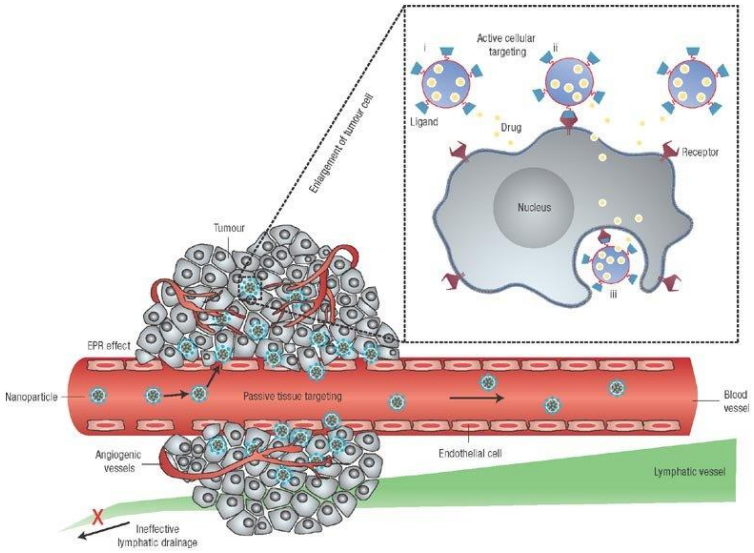

Figure 1. Nanocarriers as promising transporters of anticancer drugs to tumors by passive tissue targeting and active cellular targeting. **Passive tissue targeting** uses the increased permeability of tumor vasculature and the poor lymphatic drainage of tumors (EPR effect), allowing the release of chemotherapeutic agents in the vicinity of the tumor. **Active cellular targeting** is achieved by functionalization of the surface of nanocarriers, containing chemotherapy drugs, with targeting moieties that provide selective recognition of different receptors or antigens overexpressed in cancerous cells, increase their therapeutic efficacy, and overcomes the multiple-drug resistance. Nanocarriers, once in the vicinity of the tumor, can: (i) release their cytotoxic content next to the cancer cells; (ii) bind to the membrane of the cancer cells and release their content in a sustained way; (iii) be internalized into the cell (Peer et al., 2007).

1.1.1 Passive Targeting

Passive targeting can be attributed to the enhanced EPR effect, determined by both extravasation of macromolecules through the leaky and poorly differentiated neo-vascular tumor system and lack of functional lymphatics, which result in the accumulation of extravasated nano-

materials at the tumor site (Danhier et al., 2010; Matsumura and Maeda 1986). Typically, tumor vessels are highly disorganized and dilated with a high number of pores, resulting in enlarged gap junctions between endothelial cells and compromised lymphatic drainage. The 'leaky' vascularization, which refers to the EPR effect, allows migration of macromolecules up to 400 nm in diameter into the surrounding tumor region. In fact, as anticipated previously, the ability of vascular endothelium to present open fenestrations was widely described in inflamed tissues, in hypoxic areas of infarcted myocardium (McDonald et al., 1999; Galaup et al., 2012) or in tumors (Nagy et al., 2012). In particular, the vessels inside a tumor region are well-known for their leaky walls, allowing NPs with the right sizes to pass through efficiently. Particles, such as nanocarriers (in the size range of 10–150 nm), can easily extravasate and accumulate inside the interstitial space. Moreover, lymphatic system inside a tumor is largely absent or dysfunctional, the insufficient drainage facilitates accumulation of nanoparticles in the tumor tissue (Maeda 2001; Maeda et al., 2013; Perrault and Chan 2010). This condition further contributes to an inefficient drainage from the tumor tissue, due to an increased interstitial pressure and a reduced intra-extravascular gradient (Baronzio et al., 2012). NPs that enter into the tumor microenvironment are not removed efficiently and are thus accumulated and retained inside the tumor. Using this mechanism, a very high local concentration of drug-loaded nanocarriers can be delivered to the tumor site at, for instance, a 5–50-fold higher rate than in normal tissue within few days (Din et al., 2017). However, these approaches also suffer from several limitations, the vessels formed through angiogenesis are not evenly distributed in a solid tumor and the permeability may not be homogeneous

throughout the tumor. Targeting cancer cells using the EPR effect is not feasible in all tumors because the degree of tumor vascularization, porosity of tumor vessels and interstitial pressure can vary with the tumor type. For example, hypo vascular tumors such as prostate and pancreatic cancers are very difficult to reach. Moreover, even within a single tumor, huge differences with regard to vascular permeability can be found, with parts in which macromolecules as large as 200 nm are able to extravasate and penetrate, whereas in other parts, even molecules of about 15 nm are unable to enter the interstitium. Another limitation can be the presence of necrotic areas, especially in larger neoplasms (Rossin et al., 2005). A possible advantage for the use of small NPs (around 15 nm) could be the possibility of passive transport even inside this difficult tissue once in the interstitial fluid circulation (Huang et al., 2012). Finally, although tumor targeting consists in passive targeting and active targeting, the active targeting process cannot be separated from the passive because it occurs only after passive accumulation in tumors.

1.1.2 Active Targeting

One way to overcome the limitations of passive targeting is to attach affinity ligands (antibodies, peptides, aptamers or small molecules that only bind to specific receptors on the cell surface) to the external surface of the nanocarriers by a variety of conjugation chemistries (Arap et al., 1998; Leamon and Reddy 2004; Sudimack and Lee 2000; Wu et al., 2010). These methods can be categorized as conventional bioconjugation strategies (direct conjugation, linker chemistry, physical interactions), click chemistry or hybridization methods (Aubin-Tam 2013; Yu et al.,

2012). Furthermore, only nanosystems based on proteins allow an additional and more powerful conjugation method, i.e. the genetic engineering approach. Genetic engineering represents a much easier and more reproducible method of generating protein-based NPs with exactly the same architecture as those obtained with chemical modifications. In fact, peptide sequences can be genetically inserted into the amino acid protein sequence to build a homogenous and ready-to use construct for selective cellular recognition and thus avoid repeated and expensive chemical reactions (Vannucci et al., 2014; de la Rica and Matsui 2010). Furthermore, when NPs bind to specific receptors and then enter the cell, they are usually surrounded by endosomes via receptor-mediated endocytosis, thereby bypassing the recognition of P-glycoprotein, one of the main drug resistance mechanisms (Maeda 2001; Allen 2002). In fact, a variety of mechanisms at the cellular level contribute to drug resistance. These include the presence of drug efflux proteins on the cell membrane, an example of which is the membrane bound P-glycoprotein (P-gp), which decreases the intracellular concentration of cancer drugs (Links and Brown 1999; Krishna and Mayer 2000). P-gp may also be present on the nuclear membrane limiting drug transport into the nucleus (Calcabrini et al., 2000). Additionally, drugs showing intracellular access may be trapped in cytoplasmic vesicles, not released and then degraded, or externalized from the cell still contained in the exocytosed vesicle (Vasir and Labhasetwar 2005). Based on the receptor-mediated endocytosis mechanism, targeting conjugates bind with their receptors first, followed by plasma membrane enclosure around the ligand–receptor complex to form an endosome. The newly formed endosome is transferred to specific organelles, and drugs could be released by acidic pH or enzymes. Active targeting is mediated

by NP-conjugated ligands that are able to bind with high affinity and selectivity to target molecules over-expressed by tumor cells as compared to healthy tissues (Danhier et al., 2010; Friedman et al., 2013). Active drug targeting is generally realized to improve target cell recognition and cell uptake. Targeting ligands which have been investigated to date include peptides, small organic molecules, oligosaccharides and monoclonal antibodies (mAbs) (Friedman et al., 2013). The mAbs have been widely used as tumor-homing molecules for the targeted delivery of NPs; however, several limitations including large size, difficulty in conjugation to NPs and high manufacturing costs have hampered their use. Thus, looking to obtaining similar selectivity toward the target, NPs decorated with smaller-sized ligands (including peptides) have attracted greater attention these days (Talekar et al., 2011). In general, two cellular targets can be distinguished in the active targeting strategy: (a) the targeting of cancer cell and (b) the targeting of tumor vasculature. In the latter strategy, the nanocarriers have more chances to reach the target as it does not depend on extravasation and penetration across tumor interstitium since they encounter their target receptors much more frequently than do cancer cell targeted NPs (Sakhrani and Padh 2013; Bedi et al., 2013; Wang et al., 2011).

1.2 Drug delivery based on Nanoparticles

Multifunctional integrated systems based on NPs that combine differing properties such as tumor targeting, therapy, and imaging in an all-in-one system are providing more useful multimodal approaches in the battle against cancer. These systems have been intensively studied with the

aim to overcome limitations associated with conventional cancer diagnosis and therapy, such as rapid clearance, insolubility under aqueous conditions and lack of selectivity (Rossin et al., 2005; Bao et al., 2013; Howell et al., 2013; Chen et al., 2013). An ideal multifunctional nanocarrier would allow for the simultaneously loading of therapeutics, ligands for cell specific targeting and fluorescent materials for ease of detection. Targeting cancer therapeutics to solid tumors is facilitated by particle delivery systems capable of escaping phagocytic clearance by the reticuloendothelial system (RES) (Papisov 1998; Moghimi and Patel 1998, Aggarwal et al., 2009). Under ideal conditions such delivery systems preferentially extravasate the tumor vasculature and accumulate within the tumor microenvironment (Maruyama et al., 1999). By design, a particle delivery system capable of sequestering a cancer drug solely within a tumor may also reduce the accumulation of the drug in healthy organs (Papisov 1998; Moghimi and Patel 1998; Paciotti et al., 2005). Consequently, these delivery systems may increase the relative efficacy or safety of a cancer therapy, and thus serve to increase the drug's therapeutic index. Effective cellular drug delivery must develop methods to overcome or bypass such cellular resistance mechanisms (Shubik 1982; Jones et al., 1998; Baban et al., 1998; Hobbs et al., 1998; Jain 2001, Salmaso and Caliceti 2013). The field of nanotherapeutics has been made possible by the development of manufacturing methods that enable synthesis, self -assembly or fabrication of objects with defined size, shape and chemistry on the nanometer scale and that are also biocompatible (Kanapathipillai et al., 2014). The ideal nanocarrier size should be somewhere between 10 and 100 nm. Indeed, as discussed previously for efficient extravasation from the fenestrations in leaky vasculature, nanocarriers should be much less than 400 nm. On the

other hand, to avoid the filtration by the kidneys, nanocarriers need to be larger than 10 nm. The charge of the particles should be neutral o anionic for efficient evasion of the renal elimination. The nanocarriers must be hidden from the RES, which destroys any foreign material through opsonization followed by phagocytosis (Malam et al., 2009; Gullotti and Yeo 2014). For this reason, nanocarriers are frequently functionalized to protect them from the reticuloendothelial system and to increase the biocompatibility, solubility and stability in the bloodstream. The common method to do this consists of coating the surface of the particles with polyethylene glycol (PEG), a procedure called PEGylation. The coating of PEG chains to the surface of NPs results in an increase in the blood circulation half-life by several orders of magnitude (10-100) (Ferrari et al., 2013; Essa et al., 2011; Pozzi et al., 2014). In fact, by creating a hydrophilic protective layer around the NPs, steric repulsion forces repel the absorption of opsonin proteins, thereby blocking and delaying the opsonization process (Sant et al., 2008; Romberg et al., 2008; Xie et al., 2007). Several additional approaches have been devised in recent years to extend the life span of NPs by slowing their clearance from the body, such as polysaccharide dextran decoration, PASylation and CTP (carboxyl terminal peptide) conjugation (Kotagiri et al., 2013; Schlapschy et al., 2013; Fares et al., 2007, Köber et al., 2015). In particular, the last two approaches are based on recently developed technologies which involve genetic fusion or chemical conjugation with polypeptide sequences composed of the amino acids Pro, Ala, and Ser (for PASylation) or derived from the carboxyl terminal of human chorionic gonadotropin β subunit (for CTP). The use of natively disordered amino-acid PAS sequences as a biological alternative to PEG it was reported to eliminate the disadvantages

occurring in the case of protein-PEGylation for the following biopharmaceutical development and production (Schlapschy et al., 2013; Harari et al., 2014). These sequences can readily be attached to a wide array of existing proteins and material, stabilizing them in the bloodstream and greatly extending its life span without additional toxicity or loss of desired biological activity (Fares et al., 2007; Schlapschy et al., 2013). Moreover, in the case of protein-based materials, PAS or CTP-modified proteins can be manufactured using established recombinant DNA techniques in widely used protein expression systems. Hence, the benefits of these technologies are substantial decreasing manufacturing complexity or high costs. A variety of materials are used to construct a NP including ceramic, polymers, lipids, and metals. NPs used for drug delivery can be readily fabricated from either organic and polymeric or inorganic materials, with their sizes being controlled typically in the range of 1–100 nm and compositions/ structures being engineered to load anticancer drugs in a variety of configurations (Thomas et al., 2010; Lobatto et al., 2011, Hnawate and Deore 2017). Examples of biocompatible nanocarriers include those composed of liposomes, polymers, micelles, engineered multi-functional antibodies, and nanoparticles that can be composed of metals (e.g., gold, silver), polymer, quantum dots, dendrimers, fullerenes, proteins, DNA, other biological molecules or combinations of these materials (Nie et al., 2007; Alexis et al., 2010; Lammers et al., 2012; Ding et al., 2013).

1.3 Protein-Based Systems

Protein-based nanocarriers are attracting growing interest due to their exceptional characteristics, namely biodegradability, solubility, functionalization versatility and their extraordinary binding capacity to various drugs. A protein-based nanomedicine platform utilizes natural or synthetic protein as a template for the production of a different multifunctional nanosystem (Lee and Wang 2006). A variety of proteins have been used and characterized for drug delivery including viral capsids, monoclonal antibodies, heat shock proteins (Hsp), albumin, transferrin and ferritin (Ft) (**Figure 2**). In the recent years, protein-based nanocarriers have shown a tremendous potential for targeted delivery of drugs to cancer cells. Recombinant antibodies loaded with drugs, also called antibody-drugs conjugates (ADCs), have been investigated due to their high target specificity, and an extensive pharmaceutical development is ongoing (Birrer et al., 2019; Carter and Lazar 2018). Beyond antibodies, a small number of proteins stably circulating in the human blood have been considered as potential alternatives for drug delivery, mainly serum albumin (Park et al., 2012), transferrin (Daniels et al., 2012) and ferritin proteins (Fan et al., 2013). These three proteins are physiologically internalized through specific membrane receptors that are over-expressed on cancer cells. Within the three, ferritin is that one best classifying as a drug nanocarrier, due to its structural and biochemical peculiarities.

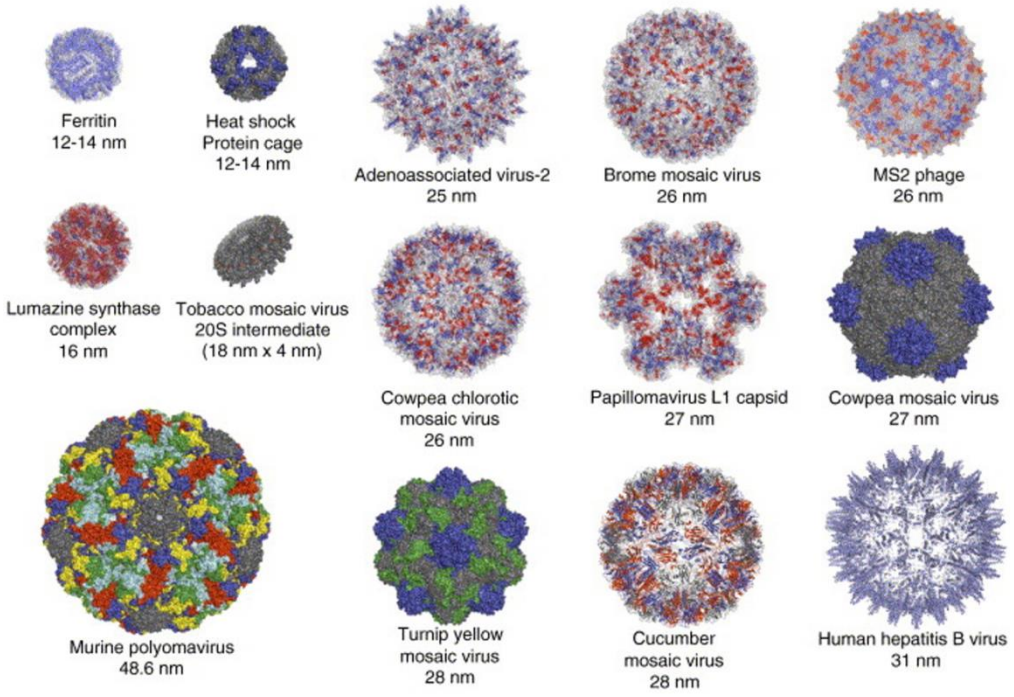

Figure 2. Types of protein cage structures currently being developed for applications in bionanotechnology applications.

1.4 Ferritins

Ferritin describes a family of iron storage proteins with ubiquitous distribution among all life forms, with the notable exception of yeast vertebrate and they are the most abundant members of the ferritin-like superfamily (Crichton and Boelaert, 2009).

1.4.1 Structural and functional properties

Ferritin consists of 24 subunits that form a globular protein, assemble into a shell-like molecule enclosing a hollow cavity with external

and internal diameters of 12 nm and 8 nm, respectively (Harrison and Arosio 1996). A non-toxic, water soluble, yet bioavailable iron core, often consisting in a ferric oxy-hydroxide mineral, is stored within the ferritin hollow shell. Ferritin protein without loaded iron is also referred as apoferritin (Ceci et al., 2012). The single subunits of the 24-mer cage of all these proteins are folded in a characteristic four-helical bundle, formed by four antiparallel helices (A-D, named in order from the amino terminus), and a shorter helix on the top of them (E) in the carboxy-terminal end lying at a 60° angle with respect to the four-helix bundle (**Figure 3**).

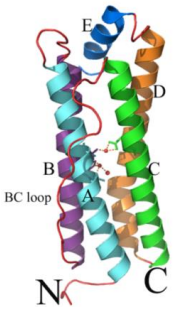

Figure 3. Monomeric fold of Human H ferritin.

The subunits related by 3- and 4-fold symmetry form at their junction pores that traverse the protein shell so as to allow the passage of ions and small molecules (**Figure 4**).

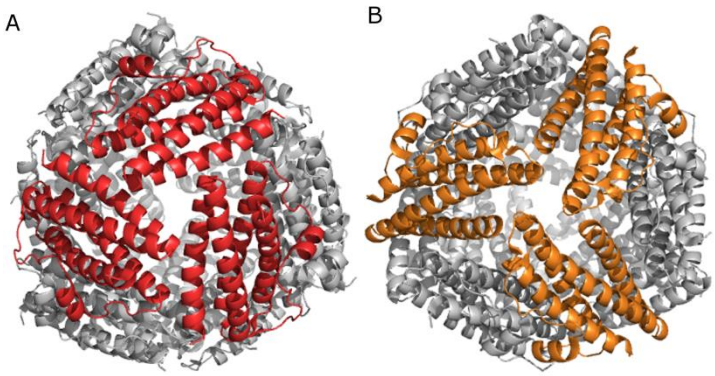

Figure 4. Quaternary assembly of ferritin from *Pyrococcus furiosus* (PDB code: 2JD7). **A.** View along the four-fold axis. **B.** View along the three-fold axis. The subunits forming the four- and three-fold interfaces are indicated in orange and red, respectively, the other subunits are grey.

The threefold pores are hydrophilic, being lined with negatively charged residues, and are involved in the uptake of Fe(II) ions. Iron in particular is guided to the 3-fold pores by a negative electrostatic gradient, enters the channels and reaches specific catalytic sites, named the ferroxidase sites, where it is oxidized by molecular oxygen. Fe(III) thus produced moves to the protein cavity where the iron core nucleates and grows at specific iron binding/nucleation sites to encompass up to 4,000 iron atoms (**Figure 5**).

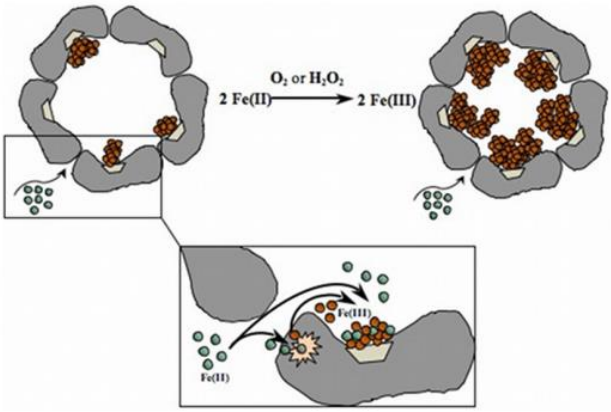

Figure 5. A schematic illustration of the most widely accepted mechanism for iron incorporation in ferritin proteins. Briefly, Fe(II) atoms (green) enter the cavity enclosed by protein subunits (dark grey) *via* the hydrophilic pores. From these pores, Fe(II) atoms are driven to the ferroxidase centre (light pink) where they are oxidized to Fe(III). Fe(III) atoms (brown) move to the iron nucleation sites (light grey), where Fe(III)-mineral formation is initiated. When the Fe(III)-mineral reaches a sufficient size, Fe(II) atoms can also get oxidized directly on the surface of the growing mineral.

All animal ferritins are assembled from two subunit types, the heavy (H chain; 21 kDa) and light chains (L chain; 20 kDa); H chains contain the catalytic centers and are more abundant in tissues with an active iron metabolism. L chains contain many nucleation sites and are more abundant in iron storage tissues like spleen (horse spleen ferritin, for example contains ~15% H and ~ 85% L chains). In contrast, bacterial ferritins contain a single subunit type that resembles the H chains. The quaternary structure of ferritin (i.e., the globular protein shell) is well-conserved. The N-terminal ends of each subunit are located on the ferritin surface and the C-terminal ends point toward the inner cavity **(Figure 6)**.

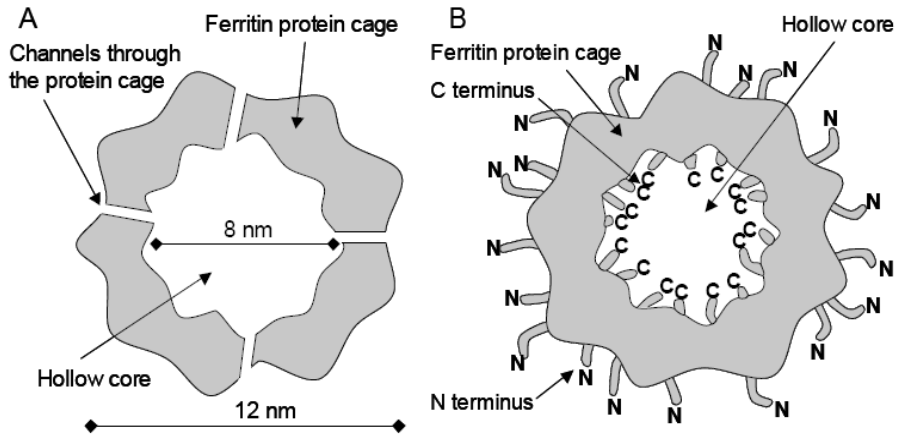

Figure 6. Schematic representations of ferritin (cross section). **A.** Ferritin is globular, hollow protein with outer and inner diameters of 12 nm and 8 nm, respectively. The protein coat is perforated by several small channels. **B.** Ferritin consists of 24 subunits, the amino-termini (denoted with N) of which protrude from the protein outer surface. The carboxy-termini (denoted with C) are located in the inner cavity of the protein.

1.4.2 Ferritins for human applications *in vivo*

Nanocarriers based on the heavy chain of the human protein ferritin (HFt) compare favorably with other systems, particularly for human applications *in vivo*. HFt is an ideal carrier due to its outstanding features, namely solubility, biocompatibility, biodegradability, functionalization versatility and remarkable capacity to bind different types of drugs (Jain 1999; Zhen et al., 2013; Dominguez-Vera et al., 2010; Falvo et al., 2013; Fan et al., 2012, Vannucci et al., 2012 and 2015). Additionally, HFts are able to pass body barriers and, being natural self-constituents, they are likely not to elicit strong non-self antibody and/or T cell immune responses. Indeed, HFts are present, under physiological conditions, both

inside cells and, although at low levels (about 20 µg/L), in the bloodstream, where they are stable and soluble. Of particular relevance, especially in view of potential applications in cancer therapy, is the ability of HFt to be easily internalized by many types of protein- and iron-hungry cancer cells (Li et al., 2010) thanks to the presence of a specific, highly overexpressed, H-ferritin receptor (see below). Furthermore, the well-conserved structure of ferritin is responsible for several characteristics that make the protein an intriguing material for biotechnology applications. The exceptional stability of the Ft cage structure over a wide range of temperatures (up to 80 °C) and pH (2–10) makes large scale production at a low cost through recombination techniques possible, and high yield (grams or even kilograms). The sensitivity of the stable cage-like structure of ferritin to pH facilitates the application of various drug-loading methods. For example, under extreme environments, such as strong acidic pH, the quaternary structure of ferritin disassembles but, interestingly, reassembles once pH returns to physiological conditions. Thus, by manipulating the disassembly and reassembly of ferritin, it is possible to encapsulate therapeutic drugs inside its structure (**Figure 7**). In fact, due to its 8-nm diameter inner cavity, ferritin has the potential space to encapsulate many drug molecules, thus offering protection from degradation as well as limiting potential side effects to healthy cells.

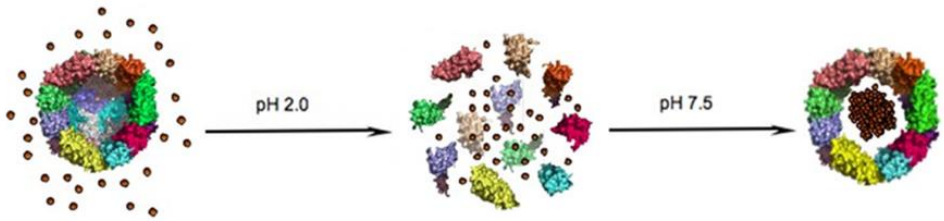

Figure 7. Schematic illustration of nanoparticles synthesis using ferritins as nano-reactors (see text for details). Ferritin-drug loading approach using the assembly-disassembly approach.

The dimension of the HFt is an important feature of this protein cage. In fact, the HFt small size (<20 nm) increases the chances of passing human body barriers and reaching specific targets. Indeed, the dimensions of the NPs, which must be small enough to penetrate capillary fenestrations and large enough to avoid rapid clearance through the kidney (the ideal diameter being lower than 30 nm and greater than 6–8 nm, respectively), are one of the key prerequisites for efficient targeted delivery, together with a long-circulating capability of the carrier and high specificity of the selector towards the target receptor. Additionally, HFt can be easily functionalized through genetic engineering and/or chemical conjugation involving one of the many chemical groups naturally exposed to the protein exterior (primary amines, carboxylates, thiols). In this way, the exterior surface is another platform to be used for drugs loading, such as chemotherapeutics, toxins and cytotoxic peptides. However, at present a

few studies have begun to design the external surface of ferritin NPs as a carrier to deliver drugs for the purpose of therapy (Kwon et al., 2012).

1.4.3 Tumor Targeting Using Ferritin-Based NPs

For drug-delivery applications, the development of molecules endowed with the ability to specifically direct NPs to selected cells and tissues would be of great value. In this direction, the exterior surface of the ferritin assembly possesses all the features necessary to operate as an appropriate platform for specific cell targeting/delivery. As mentioned above, modification of the protein exterior surface can be achieved either chemically or genetically (**Figure 8**). Several examples are present in literature where human ferritin was chemically or genetically modified to produce an efficient drug-delivery system (Khoshnejad et al., 2018).

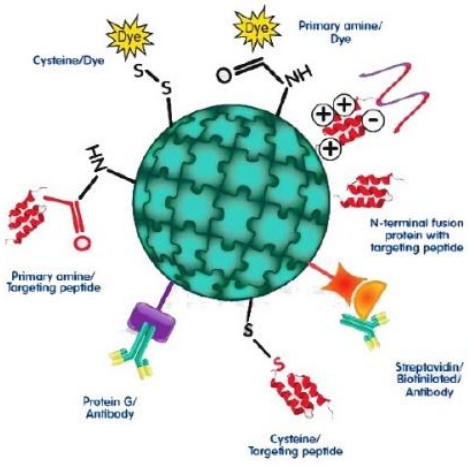

Figure 8. Ferritin external surface can be functionalized by attaching different molecules chemically or genetically (Truffi et al., 2016).

1.4.4 Intrinsic targeting ability of HFt: the transferrin receptor 1 (TfR1/CD71)

Transferrin receptor 1 (TfR1; in humans hTfR1 or CD71) is a universally expressed cell entry carrier whose primary function is to import Transferrin-bound iron in response to variations in intracellular concentration of this essential element (Gammella et al., 2017). It's a homodimeric type II transmembrane protein composed of a small cytoplasmic domain (in humans, residues 1-60), a single-pass transmembrane region (residues 61-88), and a dimeric extracellular domain (residues 89-760). Each monomer of the ectodomain, whose total molecular weight is 150 kDa, is in turn subdivided in a protease-like domain (P) in contact with the cell membrane, a helical domain (H) comprising the dimer contact regions, and an apical (A) domain (Lawrence et al., 1999) (**Figure 9**).

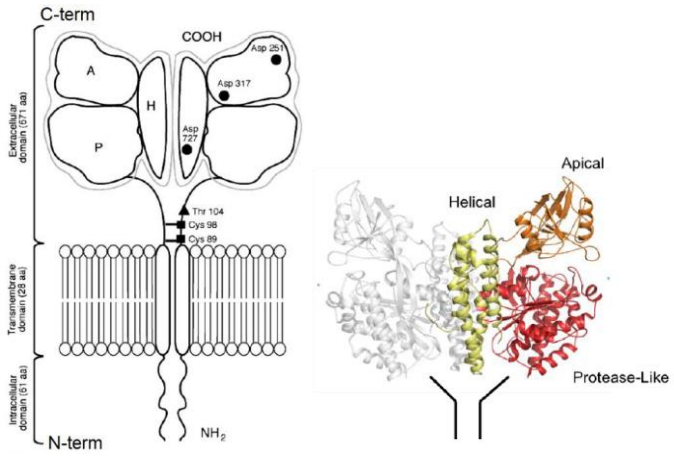

Figure 9. Human Transferrin Receptor 1 (hTfR1 or CD71). Left: cartoon structure of the whole protein, divided in intracellular, transmembrane and extracellular domains

(Daniels et al., 2012). Right: crystallographic structure (pdb 3KAS, visualized with Chimera (Pettersen et al., 2004)) of the sole ectodomain, subdivided in protease-like, helical and apical domains.

The ectodomain displays binding sites for diverse ligands (**Figure 10**). Its basal portion (formed by P and H domains) binds transferrin (Tf), while the H domain forms a complex with the Hereditary Hemochromatosis factor (HFE): these proteins are both involved in iron homeostasis. HFE negatively regulates iron uptake by competing with Tf for CD71: its association lowers the affinity of hTfR1 for Tf up to 50-fold (Bennett et al., 2000; Lebrón et al., 1998).

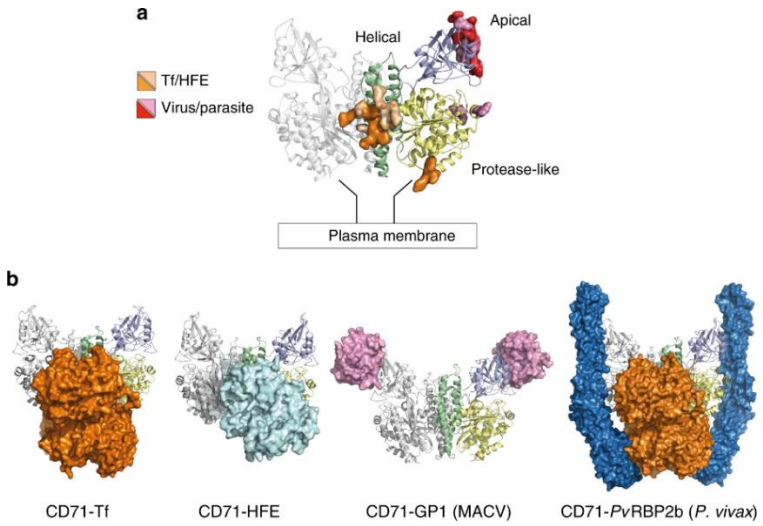

Figure 10. CD71 ligand recognition epitopes and binding modes that are to date known. A. CD71 residues identified as recognition epitopes for iron-regulating proteins Tf/HFE and viruses/parasite are represented as orange/wheat and red/pink surfaces, respectively. B. CD71 receptor is shown bound to Tf (orange surface, pdb 1SUV (Cheng et al., 2004)),

HFE (cyan surface, pdb 1DE4 (Bennett et al., 2000)), GP1 protein of MACV (pink surface, pdb 3KAS(Abraham et al., 2010)), Tf and PvRBP2b from P. vivax (orange and blue surfaces, pdb 6D04 (Gruszczyk et al., 2018)). (Figure obtained with Chimera (Pettersen et al., 2004).

Very recently, a fundamental breakthrough in the ferritin biology was reported by Li et al., (2010), the discovery that HFt *per se* has the ability to bind to CD71 and effectively target cancer cells. In fact, HFt (but not the light chain of human ferritin, LFt) was shown to be internalized by cells using the CD71 receptor. CD71 is upregulated on the surface of many cancer types (up to 100-fold higher than in normal cells) due to its involvement in iron homeostasis and cell growth regulation (**Figure 11**).

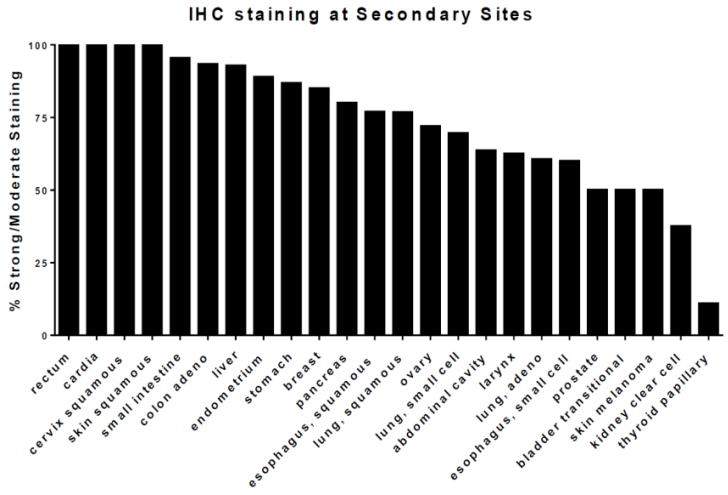

Figure 11. CD71 immunohistochemistry (IHC) staining in different tissues show that it is highly overexpressed in many metastatic cancers (Singh et al., 2016).

Recently, HFt was shown to be internalized by CD71 in more than 474 clinical tissue specimens and specifically recognize several types of tumor (i.e. liver, lung, pancreas, colon, cervical, ovarian, prostate, breast, sarcoma and thymus cancers) over non-tumor tissues with 98% sensitivity and 95% specificity (Fan et al., 2012). The high expression in cancer could involve the necessity of the DNA synthesis in these rapidly dividing cells through the ribonucleotide reductase enzyme. This enzyme needs of iron as a cofactor and for this reason the high expression of the TfR1 occurs in tumor cells (Daniels et al., 2006). In addition, two recent papers by Zhang et al., (2015), and Bellini et al., (2014) underline the selective capability of HFt, but not LFt to shuttle doxorubicin molecules to the cellular nucleus. In this case, HFt nanocages loaded with DOXO could behave like a "Trojan horse": called back within the nucleus for the purpose of defense it through the well-reported HFt antioxidant activity, HFt releases, instead, the cytotoxic anticancer drug directly into the most effective site of action **(Figure 12)**.

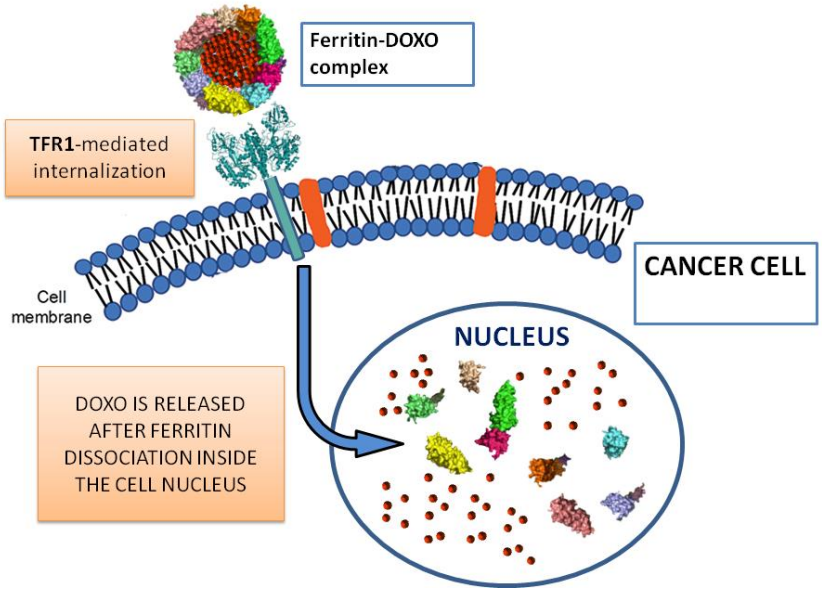

Figure 12. Schematic representation of the nuclear delivery of DOXO in HFt(DOXO) complex.

Despite the large use in literature of HFt-CD71 interaction so far discussed, the structural atomic details are to date unknown. Therefore, finding the residues involved in this contact is of major importance for providing the structural basis that govern HFt-CD71 interaction, beyond nanotechnological applications.

1.4.5 PASylated ferritins

As previously mentioned, to increase both the *in vivo* half-life of native HFt and the stability of HFt-drug complexes, our research group have developed novel HFt-based constructs, named HFt-MP-PAS, suitable

for drug delivery. In these constructs the N-terminus of each HFt subunit was genetically fused to: i) a PAS polypeptide sequence, i.e., a sequence rich in proline (P), alanine (A) and serine (S) residues; (Falvo et al., 2015, Fracasso et al., 2016) and ii) a tumor-selective sequence (MP) responsive to proteolytic cleavage by tumor proteases (MMPs), inserted between each HFt subunit and the outer PAS polypeptide (**Figure 13**).

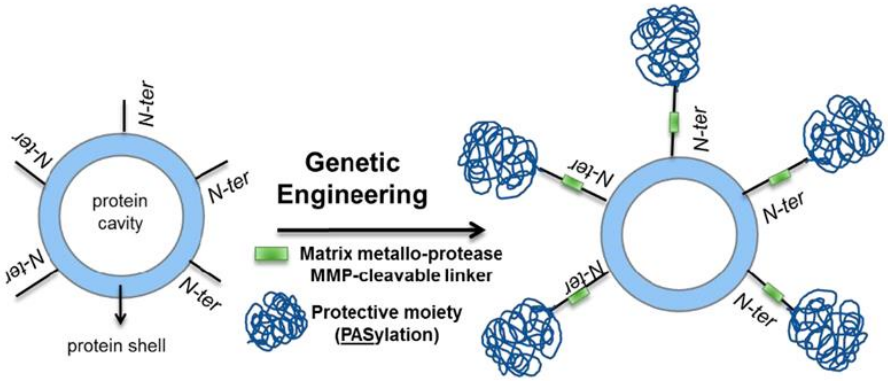

Figure 13. Schematic representation of the synthesis of HFt-MP-PAS40 (Falvo et al., 2016).

The PAS mask was aimed at hampering the interaction between drug-loaded HFt and CD71 in healthy tissues and reducing internalization by normal cells, already limited by the lower expression of the receptor. Surface plasmon resonance experiments quantified this lower interaction between PAS-masked HFt and its receptor CD71 by a factor five (Fracasso et al., 2016). Then, the MP sequence allows the PAS shield to be selectively removed by stimuli present in the tumor microenvironment (i.e., MMPs specific for this sequence) so that the resulting unmasked HFt can freely interact with and be internalized by CD71 overexpressed in cancer cells. The HFt-MP-PAS constructs proved to i) encapsulate in the internal cavity three times more doxorubicin (DOX) than wild-type HFt, ii) form more

stable complexes (i.e., drug leakage was negligible) and iii) possess higher in vivo circulation time. Importantly, DOX-loaded HFt-MP-PAS (HFt-MP-PAS-DOX) displayed excellent therapeutic efficacy either in a human pancreatic and a head and neck cancer models in vivo, significantly increasing overall animal survival (Fracasso et al., 2016, Damiani et al., 2017). We ascribed to the PAS shield the increase in DOX encapsulation, protein-drug complex stability and circulation time with respect to HFt. The higher *in vivo* efficacy of HFt-MP-PAS-DOX with respect to other DOX delivery systems is likely due to both effective PAS removal by tumor specific MMPs and efficient DOX delivery into the cell nucleus, as revealed by confocal microscopy studies (Fracasso et al., 2016). A further development in the PASylated ferritin technology would be to improve and widen the use of the HFt-based platform for drug-delivery in terms of its plasma persistence and tumor/organs accumulation *in vivo*. Some evidence suggests that the charge of NPs stemming from distinct surface chemistries influences opsonization, circulation times and interaction with resident macrophages of organs comprising the mononuclear phagocyte system (MPS), with slightly negatively charged NPs have longer circulation lifetimes and less accumulation in liver and spleen organs of the MPS (Xiao et al., 2011). This reduced binding of membrane receptors can be due to the fact that most cell surfaces, as well as extracellular matrix components, are negatively charged, too. For these reasons, our research group decided to redesign our HFt-MP-PAS carrier introducing negatively charged residues in the PAS polypeptide sequence. In particular, we genetically re-engineered HFt-MP-PAS by adding glutamate residues (E) in the PAS sequence and obtained a new construct, named HFt-MP-PASE (Falvo et al., 2018). Thanks to this modification, a 10/15-fold drop in CD71

binding affinity (a factor 3 with respect to the HFt-MP-PAS construct) was observed as determined by surface plasmon resonance experiments. This resulted in a significant improvement of the plasma persistence and tumor accumulation in a xenogenic human pancreatic cancer model (PaCa44) *in vivo* of the HFt-MP-PASE construct. Moreover, HFt-MP-PASE efficiently encapsulates the anti-cancer drug mitoxantrone (MIT). MIT is a synthetic anthracenedione developed to improve the therapeutic profile of anthracyclines and a clinically well-established anticancer agent which targets DNA topoisomerase I and ubiquitin-specific peptidase 11 (USP11) enzyme, a component of the DNA repair complex. The resulting MIT-loaded nanoparticles (HFt-MP-PASE-MIT) proved to be more soluble and monodispersed than the HFt-MP-PAS counterparts (Falvo et al., 2018). Therefore, further studies, *in vitro* and *in vivo*, would be useful in order to evaluate the real therapeutic efficacy of this new nanocarrier formulation.

2. AIMS OF THE WORK

Human ferritin H-chain (HFt) nanoparticles represent one of the most appropriate vectors for cellular delivery of molecules thanks to their internalization by CD71 (Li et al., 2010), a transmembrane receptor overexpressed in most cancer cell types (**Figure 11**). The first aim of this PhD thesis is the determination of the residues involved in the complex between HFt and the human Transferrin Receptor 1 (hTfR1 or CD71) to generate potentially more effective future constructs. The two proteins have been shown to interact very tightly: Surface Plasmon Resonance (SPR) data proved their nanomolar affinity (Fracasso et al., 2016). As such, literature is continuously enriched by successful biomedical applications of this interaction, in particular for cancer treatment (Tortorella and Karagiannis 2014; Fracasso et al., 2016; Zhen et al., 2013; Lei et al., 2016; Falvo et al., 2013). Nevertheless, the epitopes of their recognition are to date unknown.

The second aim of this thesis is to expand the interesting preliminary results obtained by our research group on the HFt-based nanovector containing Mitoxantrone (MIT) as drug payload (HFt-MP-PASE-MIT), especially in terms of *in vivo* biodistribution (Falvo et al., 2018). For this reason, we decided to deepen the characterization of this promising nanovector. In particular, the key point of this second aim is to analyze the mechanism of action and subsequently the *in vitro* and *in vivo* activity of this new ferritin–drug complex.

The last aim of this PhD thesis is to evaluate a different drug payload, more potent and versatile than those previously used by our group, like cisplatin, Doxorubic and Mitoxantrone. The drug selected by our group is named Genz-

644282, which is a non-camptothecin topoisomerase I inhibitor that shows potent activities against a large number of human tumor cell lines, with IC50s ranging from 1.8 nM to 1.8 uM (Kurtzberg et al., 2011). In addition, Genz-644282 is cytotoxic on camptothecin-resistant human cancer cell lines (Sooryakumar et al., 2011). Therefore, to allow an efficient encapsulation of Genz-644282 by the HFt nanovector, we have designed a new variant named THE-05, containing specially designed genetic point mutations in the internal surface of the protein. In this way it is possible to encapsulate weakly positively charged molecules like Genz-644282 inside the newly-designed, more negative, internal cavity of the protein.

Overall, the work of this thesis investigated the following aspects:

1. Design, production and purification of the HFt-based genetic variants as recombinant proteins expressed in *Escherichia coli.*
2. Biophysical characterization of the HFt variants using different biophysical techniques like size-exclusion chromatography (SEC), dynamic light scattering (DLS), and transmission electron microscopy (TEM) and cryo-EM (HFt-CD71 complex).
3. Assessment of the drug (MIT or Genz-644282) encapsulation yields and ferritin-drug complex stability.
4. Assessment of the binding properties and cytotoxic effect of the HFt derivatives *in vitro*.
5. Assessment of the anti-tumor and toxicity effects of the HFt-based construct *in vivo*, in mouse models of pancreatic cancer.

3. MATERIALS AND METHODS

3.1 Protein structure analysis and modeling

The atomic structure of human ferritin H-type (HFt) was downloaded from the Protein Data Bank (www.pdb.org). Protein structure visualization and modeling of PASE chains, and Gly-rich linker were performed using the software InsightII (Accelrys Inc).

3.1.1 Cloning, expression and purification of Human HFt, LFt and Mutants A, B, C, D

The genes encoding HFt and mutants A (Q14A/D15A/R22A) and B (F81A/Q83A), human apo-L-chain ferritin (Hum LFt or LFt) and its mutant D (S5T/T14Q/S22R/L81F/D116E/A119K/A123D following H-Ft numbering), were designed, synthesized, optimized for *Escherichia coli* codon usage and cloned in pET11b vector by Geneart (Geneart AG). Mutant C (Q14A/D15A/R22A/F81A/Q83A) was produced by using the Quick Change Lightning Kit (Agilent Technologies) according to the manufacturer's instructions and using mutant A as a template. All HFt and LFt variants were expressed in *E. coli* and purified as previously reported (Falvo et al., 2016).
Briefly, *E. coli* BL21 (DE3) cells harboring recombinant plasmids were grown to OD600 0.6 at 37 °C in 1 L of ampicillin-containing Terrific Broth (TB) medium (24 g/L Yeast Extract, 12 g/L Tryptone, 12.5 g/L K2HPO4, 2.3 g/L KH2PO4) (Fisher Scientific). Gene expression was induced by addition of 0.5 mM isopropyl-1-thio-ß-D-galactopyranoside (IPTG) and cells were further

grown at 22 °C overnight. After cell harvesting, pellet was suspended in 50mM Tris–HCl, 0.5mM dithiothreitol (DTT), 1mM ethylenediaminetetra-acetic acid (EDTA), and 300mM NaCl, pH 7.5, and disrupted by sonication in the presence of 1mM phenylmethylsulfonyl fluoride (PMFS). The lysate was centrifuged and the supernatant containing the soluble fraction was treated 40 min at 37 °C with 0.1 mg/mL DNase supplied with 10mM MgCl2, heated to 55 °C for 8 min, and then centrifuged to remove denatured proteins. The recovered supernatant was heated a second time to 72 °C for 8 min, and then centrifuged. The recovered supernatant was precipitated in 75% ammonium sulfate. The pellet was resuspended and dialyzed overnight against phosphate-buffered saline (PBS) pH 7.5 and then loaded on a strong anion-exchange column, HiTrap Q Sepharose High Performance (GE Healthcare) previously equilibrated with the same buffer. In these conditions, HFt samples eluted from the column, whereas other *E. coli* proteins and DNA contaminants did not. The recovered HFt (or LFt) samples were ultracentrifugated at 35,000 rpm for 55 min at 6 °C using a BeckmanL8-70M ultracentrifuge (Beckman Coultier). The sample was concentrated by means of 30 kDa Amicon Ultra-15 centrifugal filter devices (Millipore, Billerica). Finally, the nanocages were sterile filtered and stored at 4 °C. Typical yields were 100 mg of pure proteins per 1 L of bacteria culture. The purity of all the preparations was assessed by SDS-PAGE (Sodium Dodecyl Sulphate - PolyAcrylamide Gel Electrophoresis), running the nanocages on 15% gels and staining the protein with Coomassie brilliant blue. Protein concentrations were determined spectrophotometrically at 280 nm, using a molar extinction coefficient (on a 24-mer basis) of 4.56×10^5 M^{-1} cm^{-1} or 3.82×10^5 M^{-1} cm^{-1} for HFt or LFt, respectively (ProtParam sofware, http//www.expasy.org).

3.1.2 Cloning, expression and purification of CD71

The gene encoding the ectodomain of human CD71 (residues 121-760) was amplified by PCR from the plasmid pAcGP67A-TfR (Dalton and Barton 2014) (Addgene). The BamHI/EcoRI was inserted using the Gibson cloning method and fused at the 3' of the Kozak sequence of the pα−H mammalian expression vector modified by the addition of the hydrophobic leader peptide from the baculovirus protein gp67 (pα−H BiP). An octa-histidine tag was also placed at the C-terminus of the CD71 gene. The expression plasmid pα−H BiP/TfR1 was transiently transfected in cells HEK293 from American Type Culture Collection using polyethylenimine (PEI) as transfection agent. Cells were grown in FreeStyle 293 expression media (ThermoFisher Scientific) supplemented with 1% of fetal bovine serum (FBS) at 37°C in a humidified atmosphere of 5% CO2. After 96 hours, cells were harvested and CD71 was purified from supernatants using Ni- or Co-affinity chromatography. Supernatant was filtered and incubated with the resin after addition of 50 mM sodium phosphate buffer, pH 8.0, together with 200 mM NaCl and 20 mM imidazole; 250 mM imidazole was used to elute CD71. The protein sample was stored at -80°C in 50 mM sodium phosphate, 200 mM NaCl, pH 8. Quality and quantity of purified protein was evaluated by SDS-PAGE and UV/visible spectra using the theoretical ε at 280 nm 96,260 $M^{-1}cm^{-1}$.

3.1.3 Cloning, expression and purification of HFt-MP-PASE

The expression vector pET-11a containing the HFt-MP-PASE gene was assembled by GENEART AG (Germany). The PASE sequence used was: ASPAAPAPASPA**E**PAPSAPAASPAAPAPASPA**E**PAPSAPA.

Gene synthesis was performed taking into account codon-optimization for high level expression in *E. coli*. Were introduced into *E. coli* BL21 (DE3) and sequenced by dideoxy sequencing to confirm the presence of the correct gene. *E. coli* BL21 (DE3) cells harbouring the recombinant plasmid were grown to OD_{600} 0.6 at 37 °C in 1 L of ampicillin-containing liquid TB medium. Gene expression was induced by addition of 0.5 mM IPTG and cells were further grown at 22°C over-nigh. Cells were harvested by centrifugation (6,000 rpm for 20 min) and suspended in 50 mM Tris-HCl (pH 7.5), 0.5 mM DTT, 1 mM EDTA), and 300 mM NaCl and disrupted by sonication in the presence of 1 mM PMFS. The lysate was centrifuged at 16,000 rpm for 45 min and the supernatant containing the soluble fraction was treated 40 min at 37 °C with 0.1 mg/mL DNase supplied with 10 mM $MgCl_2$, heated to 55 °C for 8 min and then centrifuged to remove denatured proteins. The recovered supernatant was heated to 72 °C for 8 min, and then centrifuged to remove denatured proteins. The recovered supernatant was precipitated using an ammonium sulphate cut at 75% saturation (w/v). The pellet was resuspended and dialyzed overnight against phosphate saline buffer (PBS) pH 7.5 and then were loaded on a strong anion exchange column HiTrap Q HP (previously equilibrated with the same buffer). In these conditions, HFt-MP-PASE samples eluted from the column whereas other *E. coli* proteins and DNA contaminants did not. The samples were pooled and concentrated, by using concentration tubes with cut-off 30 KDa Amicon Ultra-15 centrifugal filter devices, according to the manufacturer

instructions (Millipore, Billerica, MA, USA). Then the final sample was sterile filtered and stored at 4 °C. Typical yields were 100 mg of pure proteins per 1 L culture. The purity of all the preparations was assessed using Coomassie brilliant blue staining of 15% PAGE gels run in the presence of SDS. Protein concentrations were determined spectrophotometrically at 280 nm, using a molar extinction coefficient (on a 24-mer basis) of $4.56x10^5$ M^{-1} cm^{-1} (ProtParam sofware, http//www.expasy.org).

3.1.4 The-05 Construct Design and Production

To effectively encapsulate the anti-cancer drug Genz-644282, which is expected to bear positive charges at physiological pH values, we designed a variant of the previously reported HFt-MP-PASE construct (see above) with an enhanced negative charge of the HFt internal surface. To this end, we analyzed the three-dimensional (3D) structure of HFt which has been experimentally determined by X-ray crystallography (Lawson et al., 1991) and is available from the Protein Data Bank archive (PDB ID: 1FHA). Structure visualization and analysis was performed with InsightII (Accelrys Inc., San Diego, CA, US) and PyMol. We chose to introduce the negatively charged glutamic acid residue (Glu) in place of four native HFt residues, namely Lys53, Lys71, Thr135, and Lys143. These residues were selected because they satisfy the following criteria: (i) their side-chains are solvent accessible on the internal surface of the HFt cavity; (ii) they are not involved in interactions, either within the monomer or at inter-monomer interfaces, whose alteration might undermine the stability of the tertiary structure or quaternary assembly, respectively; (iii) they are not involved in metal binding at the ferroxidase center of HFt; (iv) the three Lys side-chains are positively charged, and

therefore their removal contributes to the generation of a negatively charged surface; (v) their relative distance in the 3D structure is high enough that Glu residues introduced at these positions are not expected to give rise to unfavourable interactions, either with their surrounding residues or with one another. Finally, structure superposition between mutated and wild-type HFt structures available from the PDB indicates that introduction of mutations at positions 53 (i.e., Lys53Cys, PDB ID: 4DZ0) and 143 (i.e., Lys143Cys, PDB IDs: 3ERZ, 2Z6M, 3ES3) does not determine detectable changes in either the monomer fold or multimeric assembly. The variant of the HFt-MP-PASE construct bearing the Lys53Glu, Lys71Glu, Thr135Glu and Lys143Glu mutations was named The-05. It was obtained via recombinant protein technology, as previously reported. In brief, the expression vector pET-17b containing the The-05 gene was assembled by GENEART AG (Germany). Gene synthesis was performed taking into account codon-optimization for high level expression in *Escherichia coli*. The recombinant protein The-05 was expressed in *E. coli*, purified and quantified as described for HFt-MP-PASE

3.2 Samples preparation for cryo-EM acquisition

3.2.1 CD71/HFt complex

In vitro, incubation of HFt and CD71 at different stoichiometric ratios (HFt:CD71 = 1:1, 1:12, 1:24), temperatures (37 °C, 20 °C, 4 °C) and incubation times (60', 30', overnight) results in protein aggregation due to the presence of multiple binding sites on both HFt and CD71, forming insoluble precipitates. Several attempts in the stabilization of the sample with cryo-compatible Polyethylene Glycol (PEG) at different molecular weights (PEG6000 and PEG8000) and concentrations (ranging from 1% to 5%) resulted in the same

outcome. We managed to isolate a soluble sample of CD71/HFt complex by means of a pull-down experiment, as already established (Li et al., 2010). 250 µg 8xHis-tag fused CD71 was incubated with 100 µL of TALON resin (TALON Superflow Metal Affinity Resin, Ge Healthcare) in 25 mM TrisHCl, 150 mM NaCl, 1% PEG8000 and 10 mM Imidazole, pH 7.2 (buffer A), for 60 minutes at 4°C, under rotation. After several washes with buffer A, CD71-conjugated beads were incubated with 950 µg of HFt for 90 minutes at 4°C under rotation. The beads were washed increasing imidazole concentration in buffer A up to 30 mM, and the complex was eluted in 350 µL using 290 mM imidazole in buffer A. As control, CD71-unconjugated beads were also incubated with 950 µg of HFt for 90 minutes, following the same procedure adopted to isolate the complex. The pull-down assay final samples were analyzed by SDS/PAGE.

Purified CD71/HFt complex eluted from Talon resin at 0.2 mg/mL was directly used for grid preparation. Two datasets were collected using the same batch of grids to obtain the final map.

3.2.2 Grids preparation for cryo-EM

Holey-gold R0.9/1 (dataset 1 of CD71/HFt complex) and holey-carbon R1.2/1.3 covered by 2 nm film of carbon (dataset 2 of CD71/HFt complex) grids from Quantifoil Micro Tools, GmbH, were prepared as described (Russo and Passmore 2014). Grid surfaces were treated with plasma cleaning (Fischione Instruments Plasma Cleaner) using a mixture of 75% Ar and 25% O2 for 60 s before applying 3 µl of sample. We applied the samples on the

grids using a Vitrobot Mark IV (FEI, Hillsboro) (Dubochet et al., 1998) kept at 100% humidity and 4°C.

The screening of several blotting conditions revealed that the time between sample application to the grid and plunge into ethane affects enormously the number of particles per field and their distribution: this time is indicated as "waiting time". The waiting times for the different samples were: 135 s for dataset 1 of CD71/HFt complex and 90 s for dataset 2 of CD71/HFt complex. Grids were then blotted on filter paper at force 4 for different times; this time is referred to as "blotting time". The blotting times used were: 1s for CD71/HFt complex (datasets 1 and 2). After blotting, grids were vitrified by rapidly plunging into liquid ethane at −180 °C.

3.2.3 Cryo-EM data collections and analysis

Cryo-EM data collections, analysis and structures resolution was carried-out by the group of Prof. Beatrice Vallone (Sapienza University) in collaboration with the University of Columbia (USA). The complete description of these parts is reported in the co-authored paper published in Nature Communications (Montemiglio et al., 2019).

3.3 Surface plasmon resonance (SPR)

The interactions between the immobilized N-terminal His-tagged CD71 (ligand) and HFt-based constructs (analytes) were measured by surface plasmon resonance (SPR) technique on a Biacore X100 instrument (Biacore, Uppsala, Sweden) according to the procedure previously reported (Falvo et al.,

2016). Briefly, CD71 was immobilized on a Sensor Chip nitrilotriacetic acid (NTA) (GE Healthcare Europe GmbH) according to the manufacturer's instructions. The optimal experimental setup was determined and CD71 was injected at 22 μg/ml for 60 s. Analyte concentration was in the range of 1,000–62.5 μg/ml. The sensor chip surface was regenerated using fresh histidine tagged protein after every cycle of the assay. The SPR assay was performed at 25 °C, at flow rate 30 μl/min; the association and dissociation phases were monitored for 180 and 600 s, respectively. Analytes were dissolved in degassed 10 mM PBS at pH 7.4. To regenerate the chip, complete dissociation of the complexes was achieved by the addition of 10 mM HEPES (4-(2-hydroxyethyl)-1-piperazineethanesulfonic acid), 150 mM NaCl, 350 mM EDTA and 0.005% (vol/vol) surfactant P20 (pH 8.3) for 30 sec before starting a new cycle. The kon and koff rates as well as the dissociation constant (KD) were estimated using the Biacore X100 evaluation software according to a 1:1 binding model or alternatively a heterogeneous analyte binding model. All experimental data shown in results section are reported at analyte concentration of 1 mg/ml. Fits are reported as black lines corresponding to a heterogeneous analyte binding model for wild type, Mutant A and Mutant B respectively, and to a simple 1:1 kinetic model for Mutant C.

3.4 Mitoxantrone encapsulation in the HFt-MP-PASE nanovector

Mitoxantrone, MIT (MedKoo Biosciences) was encapsulated using the HFt disassembly/reassembly procedure previously described for doxorubicin (DOX) (Falvo et al., 2015). Briefly, solutions of HFt-MP-PASE in 0.1 M NaCl were incubated for 10 min at pH 2.5 (pH adjusted with HCl). Then, MIT were

added to the solution at 250:1 molar ratio with respect to the protein. The pH was initially maintained at 2.5 for 10 min and then increased to 7.5 using NaOH. The resulting solution was stirred at room temperature for 30 min, filtered and dialyzed o.n. vs PBS at pH 7.4 to remove unbound drug. After dialysis, solutions were centrifuged at 15,000 rpm for 30 min at 4°C. Supernatant was collected, concentrated with 30 kDa Amicon Ultra-15 centrifugal devices, sterile filtered and stored at 4°C in the dark. HFt and MIT content of the samples was determined by the Lowry method and UV-vis spectroscopy, respectively, after extracting MIT in 1 N HCl, 95% ethanol. MIT was quantified by using the calculated molar extinction coefficient ε = 19,200 $M^{-1}cm^{-1}$ at 610 nm.

3.5 Genz-644282 encapsulation in the The-05 nanovector

Genz-644282 Trifluoroacetic acid (TFA) salt (MedKoo Biosciences) was encapsulated in The-05 using the ferritin disassembly/reassembly procedure previously described for other drugs resulting in a 120:1 molar ratio between the drug and The-05 protein (Falvo et al., 2018). The final product was named The-0504. Briefly, solutions of The-05 (2 mg/mL) in 15 mM NaCl was incubated for 10 min at pH 3.1 (pH adjusted with HCl). Protein disassembly/reassembly was achieved by dropwise addition of NaOH to pH = 7.5. After 20 min of stirring at room temperature, the product was filtered to eliminate insoluble particles. An excess of unbound drug was removed using 100 kDa Amicon Ultra-15 centrifugal devices, in 20 mM Tris-HCl at pH 7.5. Finally, the solution was sterile filtered and stored at 2–8°C in the dark. The obtained system, made of The-05 containing Genz-644282 in the internal

cavity, was named The-0504. Genz-644282 content of the samples was determined by UV-vis spectroscopy, after extracting the drug in 0.1 N HCl. Genz-644282 was quantified by using the calculated molar extinction coefficient $\varepsilon = 10{,}000\ M^{-1}\ cm^{-1}$ at 345 nm, with a linearity comprises between 0.25–0.45 AU. Protein content was also determined by UV-vis spectroscopy applying the following correction for the Absorbance at 280 nm: A280nm - (A345nm x 4.2). The-0504 was stored as lyophilized powder at 2–8C and checked monthly for its stability. The-0504 production and formulation process development studies were carried-out in collaboration with Thena Biotech and BSP pharmaceuticals (Latina, Italy).

3.6 Size exclusion chromatography (SEC) and dynamic light scattering (DLS) analyses

SEC experiments were performed using a Superose 6 gel-filtration column equilibrated with PBS at pH 7.4.

DLS experiments were carried out using a Zetasizer Nano S (Malvern Instruments) equipped with a 4 mW He–Ne laser (633 nm), as previously described (Falvo et al., 2018). Briefly, the measurements were performed at 25°C, at an angle of 173° with respect to the incident beam. The average hydrodynamic diameters (Z-average diameter) of the scattering particles were calculated using peak intensity analyses. Results are the average of at least five measurements. Empty (HFt-MP-PASE and The-05) or drug-loaded (HFt-MP-PASE-MIT and The-0504) proteins were prepared at 1 mg/mL in diluted PBS (1:2) either for SEC and DLS analyses. All the traces for SEC and DLS

experiments were analyzed with the software Origin 8.0 (Originlab Corporation).

3.7 Transmission Electron Microscopy (TEM) analysis of The-05 and The-0504

In TEM experiments, an aliquot (8 µL) of empty (The-05) or drug-loaded (The-0504) protein (0.1 mg/mL) was dispersed on carbon coated glow discharged copper grids. Sample adsorption on carbon film was allowed for about 5 min, and sample excess was adsorbed with filter paper. Then, staining with 2% uranyl acetate solution was performed for about 30 s in the dark at room temperature; staining excess was adsorbed with filter paper and the grid washed with ultrapure water. Grids were then air dried for 1h before observation at room temperature. Transmission electron micrographs were collected working with a voltage of 120 keV at a magnification of 30,000 (Libra 120, Carl Zeiss AG).

3.8 Antiproliferative effects *in vitro* of HFt-MP-PASE-MIT and The-0504

The *in vitro* cytotoxicity studies were carried-out in collaboration with Dr. Giulio Fracasso (University of Verona) and Dr. Gianluca Sala (University of Chieti).

3.8.1 The *in vitro* viability XTT assays of HFt-MP-PASE-MIT

Human pancreatic cancer cells (PaCa44) were grown in Dulbecco's Modified Eagle Medium. The growth medium was added with 2 mM glutamine, 10% of FBS and antibiotics. Cancer cells (5,000 cells) were seeded

in 90 µL of complete medium in 96- well culture microplates. The day after, cells were incubated in triplicate with 10 µL of serial dilution of Gemcitabine (GEM), free MIT or HFt-MP-PASE-MIT. After 48 h of incubation at 37°C with drugs, the medium was replaced with fresh medium w/o phenol red supplemented with XTT (2,3-Bis-(2-Methoxy-4-Nitro-5-Sulfophenyl)-2H-Tetrazolium- 5-Carboxanilide) reagent (Sigma-Aldrich, St Louis, MO, USA), according to the manufacturer's instructions. Finally, after a variable time ranging from 1 to 3 hours of incubation at 37°C cell viability was measured at 450 nm by a microplate reader (VERSAmax, Molecular Devices). The percentage of cell viability was estimated by comparing cells treated to mock treated ones. To compare the killing efficacy, we evaluated the IC50, i.e., the compound concentration yielding 50% cell viability. Kinetic intoxication viability assays were performed applying quite the same procedures described above. The only variations are the fixed drug concentrations used in the assays (i.e. 1 µM and 0.1 µM of MIT for both loaded-MIT and free MIT) and the choice to analyze the killing efficacy at different time points (i.e. 24, 48, 72 and 96 h of treatment).

3.8.2 Apotosis evaluation by flow cytometry for tumor cells treated with HFt-MP-PASE-MIT and MIT

PaCa44 cells, cells were plated (i.e. 150,000 cells) one day before in 24 well plates; the day after cells were incubated for 48 h, with the HFt loaded MIT or MIT alone at the MIT concentration of 0.5 µM for both treatments. As control we used Gemcitabine (GEM), a drug currently applied in PC therapy, at a concentration of 15.2 mM (i.e. 4 mg/ml). At the end of the incubation after some washing steps, cells were detached and apoptosis was detected using the Annexin V-FITC labelled assay. Fluorescence was acquired by a

BDFACSCanto TM II (Becton Dickinson) flow cytometer and analyzed with the FACSDiva Software.

3.8.3 MIT drug uptake by tumor cells

PaCa44 cells, cells were plated (i.e. 250,000 cells) one day before in 24 well plates; the day after cells were incubated for different time points (i.e. 20, 40, 60, 90, 120 minutes), with the HFt loaded MIT or MIT alone at the same MIT concentration used in apoptosis assays (i.e. 0.5 µM of MIT for both). Uptake was evaluated after plates washing and cell detaching exploiting the MIT fluorescence in the APC channel. Finally, fluorescence took up by cells was acquired by a BDFACSCanto TM II flow cytometer.

3.8.4 Antiproliferative effects of The-0504 *in vitro*

Human colorectal (HT29) and pancreatic (MiaPaCa2 and HPAF II) cells were obtained from American Type Culture Collection; PaCa44 cells were kindly provided by Prof. A. Scarpa (Verona University, Verona, Italy). Cancer cells were passaged every 4 days using RPMI Medium. Media was supplemented with 2 mM glutamine, 10% of FBS and antibiotics. To perform the in vitro proliferation assays 5,000 cells per well were plated in 96-well culture microplates. After overnight incubation, cells were treated in triplicate with 10 µL of serial dilutions of free Genz-644282 or The-0504 for 72 h. Then, the medium was replaced with fresh medium w/o phenol red supplemented with XTT (2,3-Bis-(2-Methoxy-4-Nitro-5-Sulfophenyl)-2H-Tetrazolium-5-Carboxanilide) reagent (Sigma-Aldrich), according to manufacturer's

instructions. Finally, cells were incubated at 37°C and the developed staining measured at 450 nm by a microplate reader (VERSAmax, Molecular Devices). The percentage of cell viability was estimated by comparing cells treated with free Genz-644282 or The-0504 to mock treated cells.

3.9 Animal Models

Animal studies were performed by Dr. Giulio Fracasso (University of Verona) for MIT-based experiments and by Dr. Gianluca Sala (University of Chieti) for Genz-644282-based experiments, according to protocols approved by:

- the Institutional Animal Care and Use Committee of University of Verona and authorized from the Italian Ministry of Health (Protocols no. 128/2014-B) and were performed in accordance with the principles laid down in the European Community Council Directives (MIT experiments).
- the Institutional Animal Care and Use Committee of the University of Chieti and authorized by the Italian Ministry of Health (Protocol no. 457/2018-PR, 20 June 2018) (GENZ-644282 experiments).

3.9.1 Therapeutic evaluation of HFt-MP-PASE-MIT *in vivo*

For the xenograft model, 5-week-old female CD1 nude mice (Charles River Laboratories) were injected subcutaneously in the right flank with 4 x 10^6 PaCa44 cells resuspended in 200 µl of PBS. When subcutaneous tumor reached a volume of about 80-100 mm^3, mice were randomized in groups of

four mice and injected e.v. in the tail vein with saline, MIT or HFt-MP-PASE-MIT. The treatment dose of 1.4 mg/Kg was normalized to MIT concentration and mice were treated twice a week for three consecutive weeks for a total of 6 injections. Tumor volume was measured with a caliper and mouse weight was monitored. Moreover, mice were observed for signs of distress or pain twice a week for all the duration of the experiment. A tumor volume ≥ 1,500 mm^3 was chosen as endpoint after which mice were sacrificed. Overall survival was also evaluated.

At the end of the experimental plan of HFt-MP-PASE-MIT, animals were sacrificed by CO2 overdose, inhalated via face mask and primary tumors were explanted. Moreover, liver, lungs, kidneys and spleen were excited from each animal. All the explanted samples were fixed with buffered formalin 4% for 4 h, dehydrated in a gradient of ethanol (from 70% to 100%), and by two passages in xylene 100%. Then samples were paraffin-embedded and cut with a microtome to obtain sections of 5µm thickness. For the histological evaluation, the slices were stained with hematoxylin/eosin (Bioptica, Milan, Italy) and examined with light microscopy using an Olympus BX-51 microscope, equipped with a KY-F58 CCD camera.

3.9.2 Therapeutic evaluation of The-0504 *in vivo*

Preliminary evaluation of The-0504 therapeutic activity was carried-out using human pancreatic HPAF II cancer cells. Female, 4–6-week-old CD1 nude mice (Charles River Laboratories; Calco, LC, Italy), were injected subcutaneously in the right flank with 3 x 10^6 cells, previously resuspended in 200 µL of PBS. When subcutaneous tumors reached a volume of about 80-100

mm^3, mice were randomized in groups of six animals and injected i.v. with 200 µL of PBS, Genz-644282 or The-0504. Genz-644282 was formulated in sodium lactate buffer as previously reported (Kurtzberg et al., 2011). The treatment dose normalized to Genz-644282 concentration was 1.5 mg/Kg. Mice were treated six times, twice a week for three weeks. Tumor volume was measured using a caliper. Mice were monitored for bodyweight and clinical signs. A tumor volume of about 1,000–1,500 mm^3 was chosen as the endpoint after which mice were culled. Overall survival was also evaluated. The study period was set at 50 days from the beginning of therapy.

4. RESULTS AND DISCUSSION

4.1 Human HFt/CD71 complex

Literature is continuously supplemented with successful applications of the HFt/CD71 complex as a bio-vehicle for targeted delivery of leads/drugs; nevertheless, the epitopes of recognition of human HFt with TfR1 are unknown. The possibility of the existence of different epitopes for HFt and Tf for hTfR1 has been largely proved by a scarce competition between the two ligands for CD71 (Li et al., 2010, Sakamoto et al., 2015). In 2017 de Turris's group reported that the BC loop in the HFt subunit appears to be fundamental for this interaction (de Turris et al., 2017). During my PhD, I had the opportunity to participate in the work that led to the resolution of the structure of the HFt/CD71 complex (Montemiglio et al., 2019). We used single-particle cryo-electron microscopy to solve the structure of H-chain ferritin bound to human CD71 ectodomain to 3.9 Å resolution, unveiling the structural determinants that govern their recognition. The final refined and validated cryo-EM map, with CD71 and HFt crystallographic structures fitted in, obtained by the Montemiglio's group, is indicated in **Figure 14**.

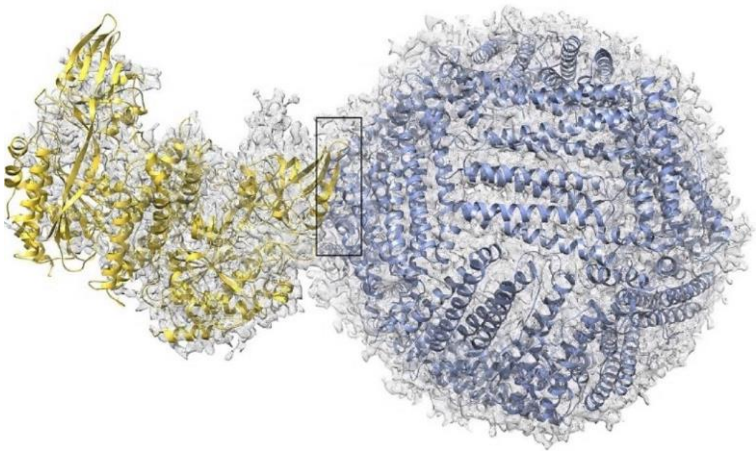

Figure 14. CD71/HFt complex final cryo-EM map (resolution 3.9 Å) with crystallographic structures fitted in (yellow: CD71, pdb 3KAS; purple: HFt, pdb 3AJO). The close-up view is in **Figure 16**.

In vitro, the combination of HFt with CD71 at different stoichiometric ratios, temperatures and incubation times results in protein aggregation. This is probably due to the presence of multiple binding sites on both HFt (24 identical subunits) and CD71 (2 subunits), that when combined form insoluble precipitates. In order to have monodisperse particles, we isolated a soluble sample of CD71/HFt complex by means of a pull-down experiment (Li et al., 2010): issues of aggregation are thus overcome (**Figure 15**).

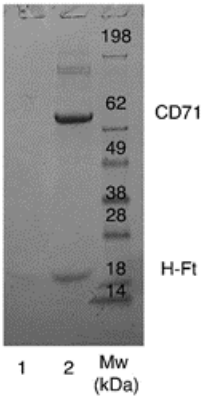

Figure 15. HFt-CD71 pull-down assay analyzed by SDS/PAGE**.** Lane 1: Beads + HFt. Lane 2: Beads-8HisCD71 + HFt. Lane 3: Molecular weights.

4.1.1 Structural analysis of the binding region

The CD71-HFt binding region is here described. HFt binds CD71 in a "virus-like" fashion, covering an overall area of ≈1900 Å2.

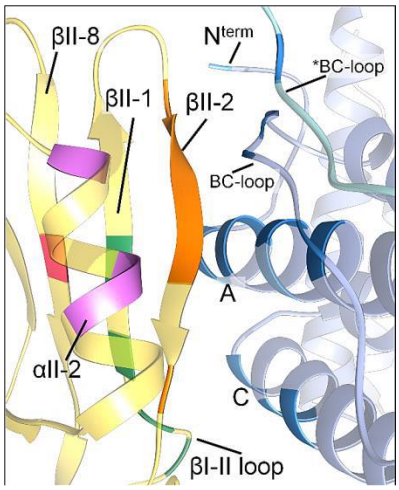

Figure 16. CD71/HFt binding region with crystallographic structures fitted in the cryo-EM map (yellow: CD71, pdb 3KAS; purple: HFt, pdb 3AJO), colored according to the text.

CD71 interacts through four specific regions on the apical domain, highlighted in different colors: i) the βI-II loop and the βII-1 strand (S195, E197, S199, I202: green); ii) a residue on the βII-8 strand (K374: magenta). These are specific on CD71 for HFt: we refer to them as "exclusive contacts". Additional residues are: iii) six amino acids on the βII-2 strand (R208-L212 and N215: orange); iv) residues E343, K344 and N348 on the αII-2 helix (purple). We refer to these as "common contacts" on CD71, since they represent the key structural determinants for binding. The HFt binding counterpart regions are three: i) the external BC loop (R79, F81, Q83, K86, K87); ii) the N-terminus of the A-helix (T5, Q14, D15, E17-A19, N21, R22, N25); iii) the C-terminus of the C helix (E116, K119, D123). An exhaustive list of HFt/CD71 pairwise contacts is given in the **Figure 18**: a summary is here briefly depicted. The interactions between exclusive contacts and HFt are: i) CD71 βII-1 strand and HFt A helix (**Figure 17 left**); ii) CD71 βI-II loop and HFt C helix (**Figure 17 left**); iii) K374 CD71 with Q14 and D15 (**Figure 17 right**).

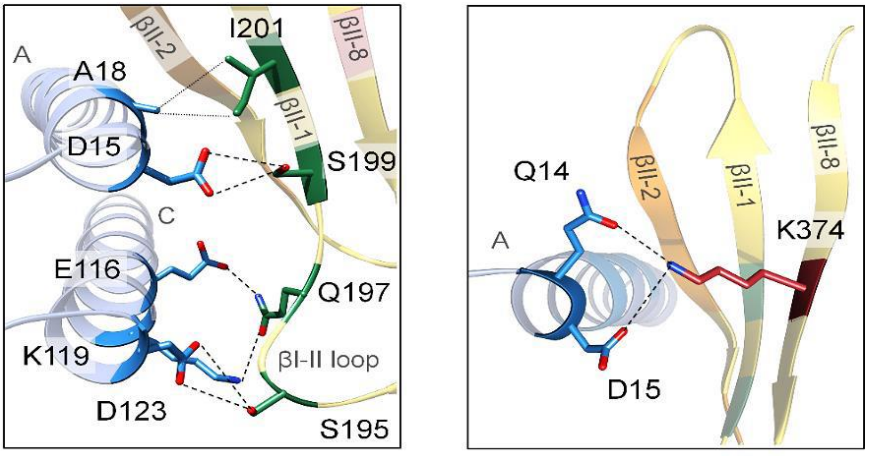

Figure 17. Contacts involving CD71 epitopes that are exclusive for HFt binding.

Notably, the CD71 amino acids belonging to “common contacts” coincide with those leading a gain or loss of interaction with pathogen binding proteins upon mutations (Gruszczyk et al., 2018, Radoshitzky et al., 2008).

*CD71	Group	Location	H-Ft	Group	Location	Distance (Å)	+exclusive/ common
Electrostatic interactions (hydrogen bonds, salt bridges)							
Ser195	OG	loop βI-1-βII-1	Asp123	OD1	helix C	4.4	exclusive
Ser195	OG	loop βI-1-βII-1	Asp123	OD2	helix C	3.7	exclusive
Gln197	OE1	loop βI-1-βII-1	Lys119	NZ	helix C	3.3	exclusive
Gln197	NE2	loop βI-1-βII-1	Glu116	OE2	helix C	4.8	exclusive
Ser199	OG	strand βII-1	Asp15	OD1	helix A	4.8	exclusive
Ser199	OG	strand βII-1	Asp15	OD2	helix A	5.0	exclusive
Arg208	NH1	loop βII-1-βII-2	Thr5	N	N-term	3.7	common
Arg208	NH2	loop βII-1-βII-2	Thr5	O	N-term	4.0	common
Arg208	NH2	loop βII-1-βII-2	Arg79	NH2	loop BC	3.6	common
Val210	O	strand βII-2	Asn21	ND2	helix A	3.0	common
Asn215	OD1	loop βII-2-βII-3	Arg22	NH1	helix A	3.3	common
Asn215	OD1	loop βII-2-βII-3	Arg22	NH2	helix A	3.3	common
Asn215	ND2	loop βII-2-βII-3	Glu116	OE1	helix C	2.7	common
Asn215	ND2	loop βII-2-βII-3	Glu116	OE2	helix C	4.0	common
Lys344	NZ	helix αII-2	Asn25	OD1	helix A	3.6	common
Gly347	O	helix αII-2	*Lys87	NZ	*loop BC	3.6	common
Asn348	OD1	helix αII-2	*Lys87	NZ	*loop BC	3.0	common
Asn348	ND2	helix αII-2	Gln83	OE1	loop BC	3.5	common
Lys374	NZ	strand βII-8	Gln14	OE1	helix A	3.4	exclusive
Lys374	NZ	strand βII-8	Asp15	OD1	helix A	5.0	exclusive

*CD71	Group	Location	H-Ft	Group	Location	Distance (Å)	+exclusive/ common
			Hydrophobic interactions				
Ile201	CD1	strand βII-1	Ala18	CB	helix A	4.2	common
Ile201	CG2	strand βII-1	Ala18	CB	helix A	4.5	common
Leu209	CD1	strand βII-2	Gln14	CG	helix A	4.5	common
Leu209	CD2	strand βII-2	Arg79	CG	loop BC	3.8	common
Val210	CG1	strand βII-2	Gln14	CB	helix A	4.8	common
Val210	CG2	strand βII-2	Glu17	CB	helix A	4.4	common
Val210	CG2	strand βII-2	Glu17	CG	helix A	4.4	common
Val210	CG2	strand βII-2	Ala18	CB	helix A	4.4	common
Tyr211	CD1	strand βII-2	Asn21	CB	helix A	3.7	common
Tyr211	CE1	strand βII-2	Gln83	CB	loop BC	4.7	common
Tyr211	CE2	strand βII-2	Gln83	CG	loop BC	3.6	common
Tyr211	CE2	strand βII-2	Gln83	CD	loop BC	4.4	common
Tyr211	CD2	strand βII-2	Gln83	CD	loop BC	4.5	common
Tyr211	CG	strand βII-2	Phe81	CD2	loop BC	4.9	common
Leu212	CB	strand βII-2	Ala18	CB	helix A	3.6	common
Leu212	CB	strand βII-2	Arg22	CB	helix A	4.2	common
Leu212	CD2	strand βII-2	Ala19	CB	helix A	4.3	common
Leu212	CG	strand βII-2	Arg22	CG	helix A	4.7	common

Figure 18. Complete list of CD71/HFt contacts.

*: The colors follow the code of Figure 16.

4.1.2 Structural analysis and design of the binding region of mutants

After the identification of the interacting region, we wanted to identify between all 17 HFt residues (DATA not shown) the crucial determinants for HFt/CD71 complex. So, amongst HFt residues involved in common contacts (T5, Q14, D15, E17-A19, N21, R22, N25, R79, F81, Q83, K86, K87, E116) we selected only those that are not conserved between human HFt and ferritins unable to bind CD71 (i.e. human LFt (Li et al., 2010) and *Archaeglobus Fulgidus* Ferritin (AfFt) (de Turris et al., 2017): they are Q14, D15, R22, F81, Q83 (black boxes in **Figure 19**). To prove their importance, we produced three multiple mutants of HFt: i) mutant A, lacking the polar residues at the N-terminal of the A helix (Q14A, D15A, R22A) ii) mutant B, lacking F81 and Q83 on the external BC-loop (F81A, Q83A) iii) mutant C, combining A and B (Q14A, D15A, R22A, F81A, Q83A).

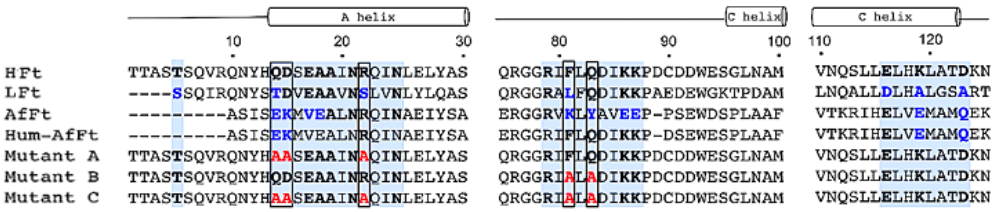

Figure 19. Ferritins (Human H and L chains, AfFt, HumAfFt, Mutants A, B, C) sequence alignment of regions contacting CD71. Elements of secondary structure are shown on the top. Colored background highlights the HFt contact regions with CD71. Conserved residues (respect to HFt) are in black, non-conserved in blue, mutated in red. Black boxes are residues crucial for CD71 binding. (Alignment made with Clustel Omega, figure with ENDscript (Robert and Gouet 2014))

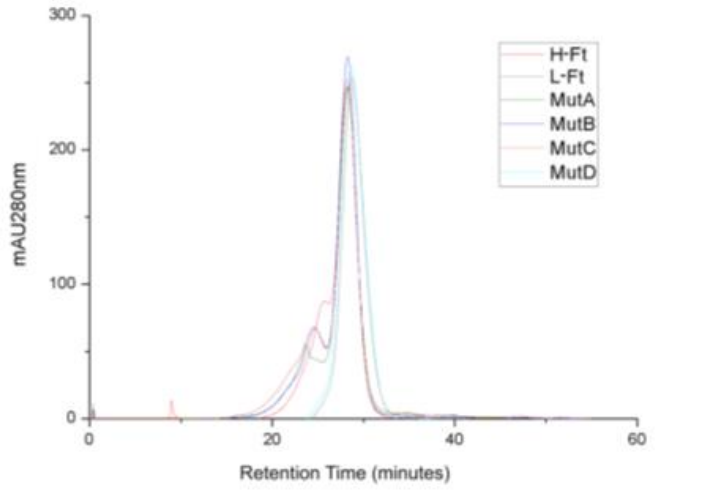

Figure 20. Gel filtration chromatographic profile of ferritins utilized in this study. A main peak at retention times typical of the human ferritin wild type (28.2 min) is present, thus proving that all mutants retain the 24-mer assembly of the human wild type ferritins. In addition, a pre-peak at about 25 min is also observed in the H-chain constructs. This was previously ascribed to the presence of cysteine residues (2 per subunit, 48 for 24-mer) on the surface of the H-chain ferritins that are absent in the L-chain proteins 2.

4.1.3 Characterization by Surface plasmon resonance (SPR)

Surface Plasmon Resonance (SPR) measurements were done to measure the kinetics (association, kon, and dissociation, koff, rates) and the affinity of the ligand-analyte interaction (KD), using wild-type or mutant HFts as analytes and CD71 as ligand. The reaction between an immobilized ligand (L) and an analyte (A) can be assumed to follow a pseudo first order kinetics; during the association phase, the complex [LA] increases as a function of time according to the following equation (Fracasso et al., 2016):

$$\frac{d[LA]}{dt} = k_{on}[L][A] - k_{off}[LA]$$

(1:1 binding model)

(heterogeneous analyte binding model)

$$\frac{d[LA]}{dt} = 2k_{on\,1}[L][A] - k_{off\,1}[LA] - k_{on\,2}[LA][L] + 2k_{off\,2}[LLA]$$

From the fit of the curves, it is thus possible to obtain a measure of kon, koff and KD of the reaction.

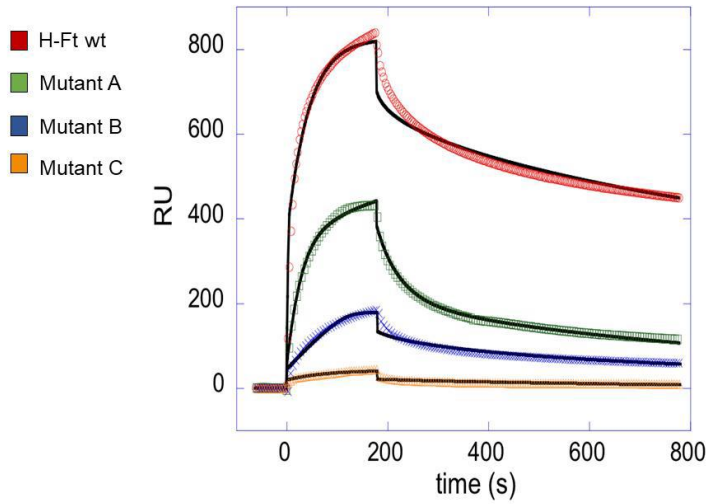

Figure 21. SPR sensograms of the interaction between the immobilized his-tagged CD71 receptor and HFts (wild-type and mutants), used as analytes. Fits are the black lines; fitted parameters are in Table 1.

The wild-type HFt-CD71 binding affinity (KD= 17.9 nM) is compatible with the one already existing in literature (Fracasso et al., 2016). Instead, this parameter is reduced of about two orders of magnitude in mutants A and B and abolished in mutant C. In particular, a critical drop of the kon value is increased

across mutants B and C, suggesting that mutations at the BC loop have a dominant role in impairing the CD71/HFt interaction: this is likely due to the loss of contact of HFt F81 and Q83 with CD71 Y211 and HFt Q83 with CD71 N348.

Table 1: Kinetic and thermodynamic parameters for SPR experiments:

Top: heterogeneous analyte fit. **Bottom**: simple 1:1 binding mode

Protein Analyte	k_{on1} ($M^{-1}s^{-1}$)	k_{off1} (s^{-1})	K_{D1} (nM)	k_{on2} ($M^{-1}s^{-1}$)	k_{off2} (s^{-1})	K_{D2} (µM)
H-Ft	$(4.78\pm0.07)*10^{5}$	$(3.40\pm0.06)*10^{-3}$	7.1±0.2	$(1.69\pm0.04)*10^{5}$	$(2.51\pm0.06)*10^{-2}$	0.156±0.007
Mutant A	$(1.1\pm0.2)*10^{6}$	$(6.5\pm0.9)*10^{-1}$	570±170	$(1.4\pm0.1)*10^{4}$	$(2.7\pm 0.1)*10^{-2}$	1.9±0.3
Mutant B	$(1.5\pm0.3)*10^{6}$	$(3.3\pm0.2)*10^{-1}$	220±80	$(1.7\pm0.2)*10^{2}$	$(2.76\pm0.04)*10^{-2}$	158±18
Mutant C	Not feasible					

Protein Analyte	k_{on1} ($M^{-1}s^{-1}$)	k_{off1} (s^{-1})	K_{D1} (nM)
H-Ft	$(3.74\pm0.08)*10^{4}$	$(6.72\pm0.08)*10^{-4}$	17.9±0.6
Mutant A	$(1.7\pm0.2)*10^{5}$	$(1.8\pm0.2)*10^{-3}$	140±50
Mutant B	$(6.6\pm0.7)*10^{4}$	$(8.9\pm0.8)*10^{-3}$	130±30
Mutant C	1200 ±100	$(1.55\pm0.03)*10^{-3}$	1300 ±100

Human LFt, which lacks Q14, R22 and F81, is unable to bind the CD71 receptor (Li et al., 2010). Notably, presents differences in seven positions (S5, T14, S22, L81, D116, A119, A123) over the total contacts required for the recognition of the receptor (see the alignment in **Figure 19** and **Figure 20**). We found that LFt to HFt mutations at these positions (mutant D) confer binding capability to CD71 with an affinity similar to the one observed for HFt (**Figure 22**).

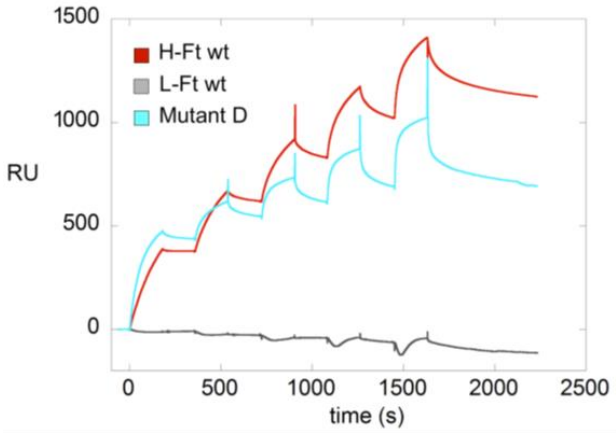

Figure 22. Single kinetic SPR assay. SPR sensograms of the interaction between the immobilized his-tagged CD71 receptor and HFt wt (red line), LFt wt (grey line) and mutant D (cyan line), used as analytes. Analyte concentration is increased in five consecutive steps from 18.75 µg/mL to 300 µg/mL. Source data are provided as a Source Data file.

4.1.4 Further considerations on HFt-CD71 binding

Importantly, up to now no other complexes associated with HFt have ever been singled out, nor the CD71 apical domain (present in all mammalians) has ever had a known physiological role. In this framework, changes due to Single Nucleotide Polimorphisms (SNPs) within CD71 apical domain may

protect from viruses or parasites entry, but cannot be considered neutral with respect to HFt uptake. Along this line, CD71 species-specific variants must conveniently match HFt co-evolved variants in order to conserve its physiological functions. For example, mouse CD71 (mCD71) apical domain is rather different from the hCD71 one in key residues for HFt binding. Indeed, mouse HFt (92% of identity with the human one (Li et al., 2010)) in mice is known to be internalized by TIM-2, that is not expressed in humans (Chen et al., 2005; Todorich et al., 2008). In literature it is still not clear whether TIM-2 is the only receptor suitable for mouse HFt or if mCD71 plays a similar role to its human counterpart. If mCD71 didn't bind mouse HFt, then iron uptake phenomenon by humans and mice organisms would be quite different, as already hinted (Li et al., 2010): proving this validation will be of great interest for iron-delivery mechanisms and to validate mice as animal models for iron-concerned researches.

4.2 Production of the HFt-MP-PASE fusion protein and the HFt-MP-PASE-MIT complex

The fusion protein HFt-MP-PASE was obtained *via* recombinant protein technology and purified (purity ≥ 95%) from the cellular soluble fraction at high yield, similar to HFt-MP-PAS (about 150 mg per liter of *E. coli* cell culture at lab scale) (Falvo et al., 2016). The drug Mitoxantrone (MIT) was encapsulated inside HFt-MP-PASE cavity following the disassembly/reassembly procedure reported in Falvo et al., 2018 (**Scheme 1**). This procedure resulted in the encapsulation of about 47 molecules (47 ± 5.0)

of the drug inside the HFt-MP-PASE cavity, with a protein recovery of about 90% (Falvo et al., 2018).

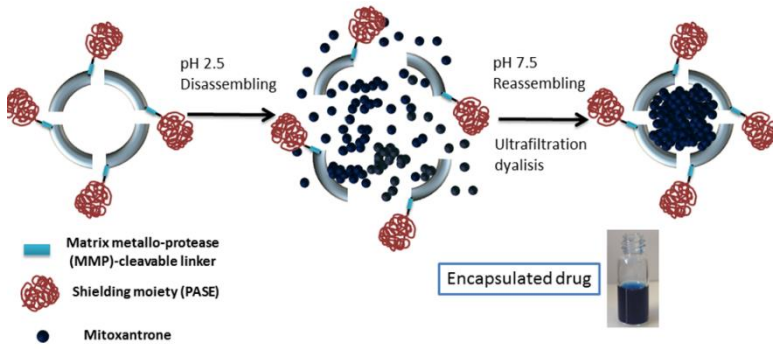

Scheme 1. Cartoon displaying the synthesis of HFt-MP-PASE-MIT. For clarity purposes, only 4 out of the 24 modified HFt N-termini are shown.

4.2.1 *In vitro* cytoxicity on PaCa44 cells of HFt-MP-PASE-MIT

Our previous results demonstrated that HFt-MP-PASE-MIT nanocages *in vitro* are efficient in killing different tumor cell lines with the same efficiency as free drug forms (Falvo et al., 2018). To confirm our observation, we first aimed in this study to test the cytotoxic capability of our generated HFt-MP-PASE-MIT on human pancreatic (PaCa44) cancer cell line given that this cell line was also used in our *in vivo* experiments. We evaluated the potency of our nano-formulation using XTT assay while collecting the data from three different experiments. As depicted in **Figure 23**, PaCa44 cells exposed to HFt-MP-PASE-MIT or free MIT for 48 h showed quite similar drug sensitivity with an IC50 drug response of 0.47 ± 0.07 µM and 1 ± 0.12 µM for loaded and free MIT concentrations, respectively. It is noteworthy that GEM,

a drug currently used in Pancreatic Cancer (PC) therapy, showed a considerably lower drug killing efficacy with IC50= 13.5 ± 1.25 mM.

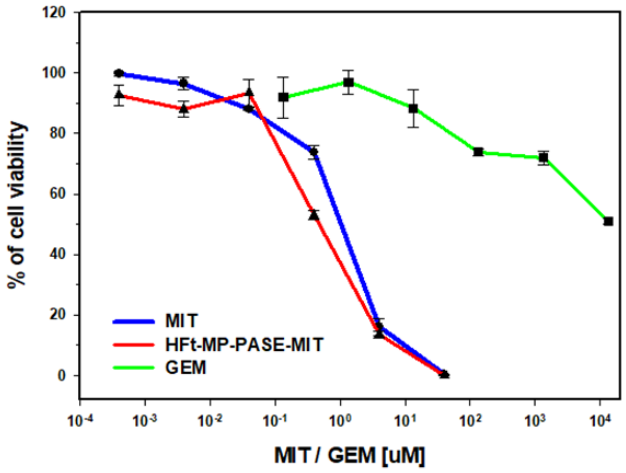

Figure 23. Cytotoxic potential of free or loaded-MIT using XTT assay. PaCa44 pancreatic tumor cells were treated 48 h with serial dilution of HFt-MP-PASE-MIT, MIT or GEM. The percentage of cell viability was measured by XTT assay, and means ± SEM were calculated from three independent experiments.

4.2.2 Flow Cytometric Analysis of Necrosis or Apoptosis

In order to identify key cellular markers of 'cell death' or apoptosis, we have measured the expression level of phosphatidylserine using flow cytometry. The Annexin V-FITC kit was employed with propidium iodide (PI) to differentiate apoptotic from necrotic cells. Annexin V has high binding affinity for phosphatidylserine proteins translocated from the inner side of the plasma membrane to its outer leaflet; while necrotic cells lost their cellular integrity and thereby are permeable to PI dye that in turn intercalates with the nuclear DNA and is visible by red fluorescence. We treated PaCa44 cells with

0.5 µM of our nano-formulation or free MIT for 48 h; GEM (4 mg/ml) that is equivalent to 15.2 mM was used as control. Results of Annexin V binding and PI uptake were quantified and summarized in **Table 2**. HFt-MP-PASE-MIT and MIT showed quite similar levels of early apoptosis 11.30% ± 1.00 and 13.25% ± 1.85, respectively. Also, the amount of cells in late apoptosis was quite similar reaching 4.95% ± 0.45 and 6.35% ± 1.05 for encapsulated and MIT-free form, respectively. Moreover, the level of cell death for necrosis was superimposable. GEM showed a similar percentage of cells in early and late apoptosis 10.01% ± 0.20 and 7.60% ± 0.50, but at a drug concentration of 15.2 mM, that is about 4 Log higher with respect to MIT concentration.

Drug concentration	Early apoptosis	Late apoptosis	Viable Cells	Necrosis
GEM 15.2 mM	10.01% ± 0.20	7.60% ± 0.50	58.00% ± 2.60	24.25% ± 2.25
MIT 0.5 µM	13.25% ± 1.85	6.35% ± 1.05	56.65% ± 1.45	23.80% ± 0.60
HFt-MP-PASE-MIT 0.5 µM	11.30% ± 1.00	4.95% ± 0.45	60.10% ± 4.90	23.70% ± 3.50

Table 2. PaCa44 cell apoptosis detected by flow cytometry after 48 h of treatment.

4.2.3 Kinetics of cell intoxication

A previous report by our group demonstrated that HFt-MP-PASE-MIT is rapidly internalized by CD71 and traffic intracellularly via the endosomal pathway. Then, loaded-MIT escapes from these organelles and arrives at the nuclear level, where MIT produces DNA breaks and cross-links. Instead, free MIT enters via passive diffusion across the plasma membrane and its

distribution is then between nucleus and cytoplasm (Falvo et al., 2018). The rate of drug uptake can directly reflect the kinetics of tumor cell killing and is pivotal in studying the efficacy of chemotherapeutic agents. In order to examine the kinetics of tumor cell death, PaCa44 cells were treated with HFt-MP-PASE-MIT or MIT alone, and subjected to XTT assays at different time points. Using an MIT normalized dose of 1 µM we observed that HFt-MP-PASE-MIT killed 1 Log of tumor cells (i.e. 90% of tumor cells) in 96 h. MIT eliminated the same amount of cells in a quite similar time of 100 h (**Figure 24**). When a ten-fold dilution of the drug was used, 0.1 µM, a slight difference was noticeable in the kinetic killing curves. HFt-MP-PASE-MIT killed 90% of tumor cells in 110 h while MIT cytotoxicity showed same killing rate at 128 h (data not shown). Moreover, the lag phase, the time elapsing before cell death, was quite over-lapping between the two drugs (i.e. 10 h for MIT and 10.5 h for HFt-MP-PASE-MIT). When the same parameter was analyzed in the killing kinetic curves obtained after treatments with a MIT concentration of 0.1 µM, HFt-MP-PASE-MIT showed a shorter lag phase compared to its free counterpart (20 h and 27 h, respectively; data not shown).

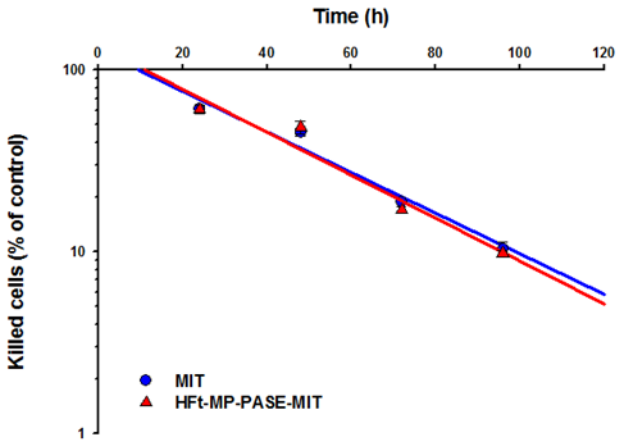

Figure 24. Kinetic curves of cell killing by HFt-MP-PASE-MIT and MIT. PaCa44 pancreatic tumor cells were treated for different time points with an equivalent MIT dose of 1 µM and viability was assessed by XTT assay. Linear regression was applied to fit the experimental data (r^2=0.97 and r^2=0.95 for MIT and HFt-MP-PASE-MIT, respectively). Three independent experiments were performed ± SEM.

4.2.4 Uptake in tumor cells

Given the comparable curves in the cell killing kinetics for both MIT forms, it was challenging to examine the rate of drug uptake especially given that encapsulated MIT molecules possess larger size and possibly different charge. To tackle our concern, we set to study the uptake of 0.5 µM of drugs by PaCa44 cells at 37°C at different time points (i.e. 20-40-60-90-120 minutes). It is worth noting that the fluorescent emission of MIT can be captured in the APC channel using flow cytometry. As summarized in **Table 3**, at all time points, HFt-MP-PASE-MIT demonstrated a superior uptake into the cells with more MIT (about 35%) accumulated in the target cells when the drug is loaded on the nanosystem.

	20 minutes	40 minutes	60 minutes	90 Minutes	120 minutes
HFt-MP-PASE-MIT vs. MIT	133.07% ± 7.21	133.25% ± 7.37	139.49% ± 6.71	142.02% ± 7.00	138.37% ± 0.74

Table 3. Percentage of the differential cellular uptake of 0.5 µM HFt-MP-PASE-MIT versus MIT at 37°C detected by flow cytometry at different time points.

4.2.5 Therapeutic efficacy *in vivo*

The *in vivo* efficacy of our nanosystem was assessed in a subcutaneous PC mouse model. PaCa44 cells (4×10^6) were injected in the left flank of 5-week-old female CD1 NUDE mice (n=4). After 16 days, when established tumors had gained a volume of about 80-100 mm^3, mice were randomized and assigned at one of the four groups (i.e. saline, free drug and encapsulated drug). Treatments were performed twice a week for three consecutive weeks by intravenous injection in the tail vein. The treatment doses were normalized to MIT dose (i.e. 1.4 mg/kg). The dose was established considering an Maximum Tolerated Dose (MTD) for MIT of 9 µmol/kg (i.e. about 4 mg/kg). So, we used about 1/3 of the MTD at each treatment for a total amount of about 8 mg that is the double of the MTD. Throughout the experiment, mice were weighted and observed twice a week for signs of distress or pain and finally they were sacrificed when the tumor gained a volume ≥ 1,500 mm^3. Tumors in control mice grew progressively, showing a tumor doubling time of about 5 days during the exponential growth phase (**Figure 25A**). Only a very limited growth delay was observed in the group treated with MIT alone, but without any

statistical significance. In contrast, we observed a high difference in tumor growth when mice were treated with HFt-MP-PASE-MIT. After an initial superimposable growth of tumor compared to mock treated animals, tumor volume started to significantly decrease when the 4th dose was administered.

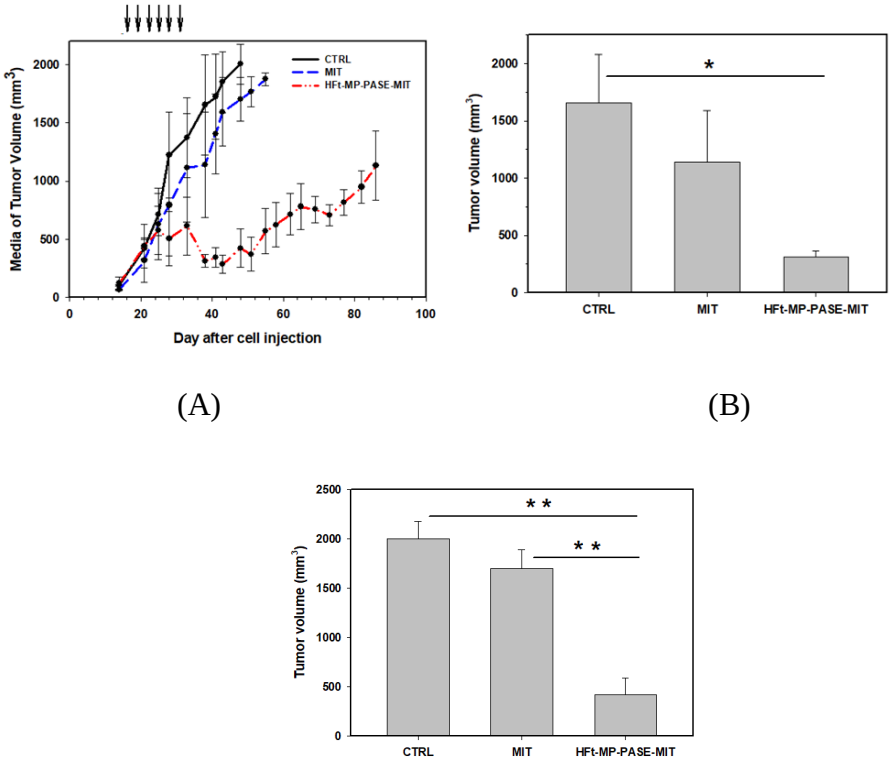

Figure 25. Efficacy of HFt-MP-PASE-MIT *in vivo*. **A)** Growth curves representing the media of the tumor volume for each of the treated groups: HFt-MP-PASE-MIT, MIT or saline (CTRL, control); n=4. Arrows indicate the six days of treatment administration. **B)** Tumor volume of the three different groups measured at day 38 after tumor cell injection. *p<0.05. **C)** Tumor volume of the three group of treated mice (HFt-MP-PASE-MIT, MIT or saline) at day 48 after tumor cell injection (n=4) *p<0.05, **p<0.01.

One week post-treatment (i.e. day 38), there was a significant difference between tumor volume of control (V=1,653.8 ± 428.5 mm^3) and HFt-MP-PASE-MIT treated mice (V=313.2 ± 54.6 mm^3, p = 0.019) (**Figure 25B**). At day 48, when the last mouse of the control group was sacrificed, the media of tumor volume between MIT (V=1,703.1 ± 189.2 mm^3 and HFt-MP-PASE-MIT (V=423.6 ± 164.4 mm^3) groups varied significantly (p=0.0075) (**Figure 25C**).

Using the Kaplan-Maier plot, mice treated with HFt-MP-PASE-MIT achieved a median survival time (OS50%) of 65 days, which is considerably greater than OS50% of 28 days and 33 days of control mice and MIT groups, respectively. Moreover, it is important to highlight the statistically significance of this increased survival (i.e. data of the Log Rank Test, HFt-MP-PASE-MIT vs. MIT p= 0.006, HFt-MP-PASE-MIT vs. control p= 0.006 and MIT vs. control p= 0.531) (**Figure 26**). Based on the p values, untreated and MIT treated groups did not show a significant improvement in the survival of mice. In contrast, encapsulated-MIT in HF-MP-PASE-MIT exhibited remarkable prolonged survival periods of almost additional 33 days compared to MIT treated groups.

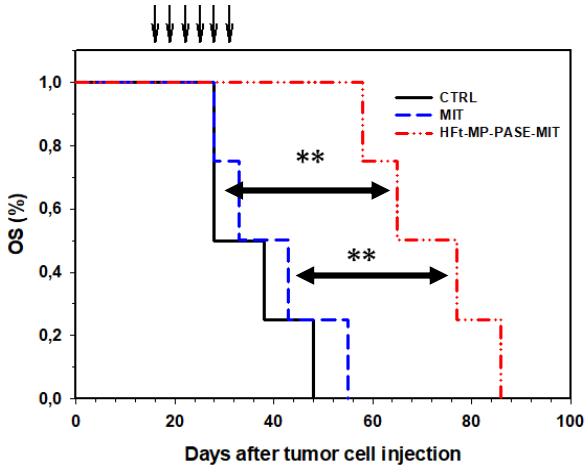

Figure 26. Kaplan-Meier survival plot. Mice with established s.c. tumor of PaCa44 cells were treated twice a week for three consecutive weeks with HFt-MP-PASE-MIT, MIT or saline (n=4) *p <0.05, **p <0.01.

Furthermore, it is important to underline that some of the mice treated with HFt-MP-PASE-MIT (i.e. 2/4, 50%) were sacrificed before reaching a tumor volume ≥ 1,500 mm^3, our abortion criteria, because the high cytotoxic activity of the drug on the tumor had created eschars (not shown). Therefore, these mice were sacrificed to not create excessive pain in the animals.

Regarding the nonspecific toxicity of our therapy, we observed that HFt-MP-PASE-MIT mice experienced a maximal weight loss of about 10% during the treatments, but then their weight was restored back to normal value (**Figure 27**) Otherwise, MIT treated mice demonstrated less capability to regain their original weight. In the same setting, control mice showed an increment in their weight of no more the 5%.

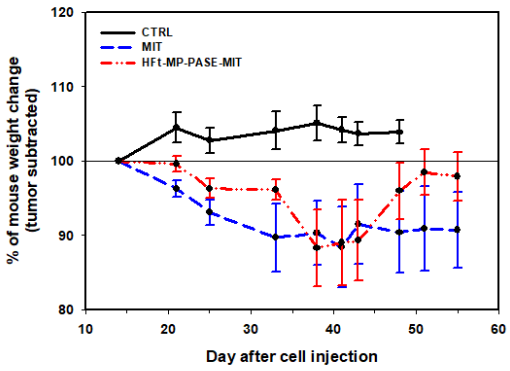

Figure 27. Percentage of mouse weight change during the treatment with HFt-MP-PASE-MIT, MIT or saline (n=4).

4.2.6 Histological evaluation of primary tumor mass

Histological evaluation of parenchyma primary tumor mass was performed using hematoxylin and eosin stain to verify the treatment efficacy of HFt-MP-PASE-MIT nanosystem. In fact, as depicted in **Figure 28A**, tumor explanted from a representative mouse belonging to the control group showed very dense parenchyma morphology typical of recta tumors with the presence of numerous capillaries. While the representative tumor, explanted from mouse belonging to the group treated with HFt-MP-PASE-MIT, showed numerous necrosis areas and scarce vascularization (**Figure 28C**). The treatment with free MIT, representing a non-targeted drug, is less efficient in reducing primary tumor viability (**Figure 28B**). Indeed, MIT administration showed a dense structure of primary tumor with rare areas of necrosis and a good presence of capillaries. Similar histological tumor mass profiles were screened for each group treatment and the selected images display representative morphologies.

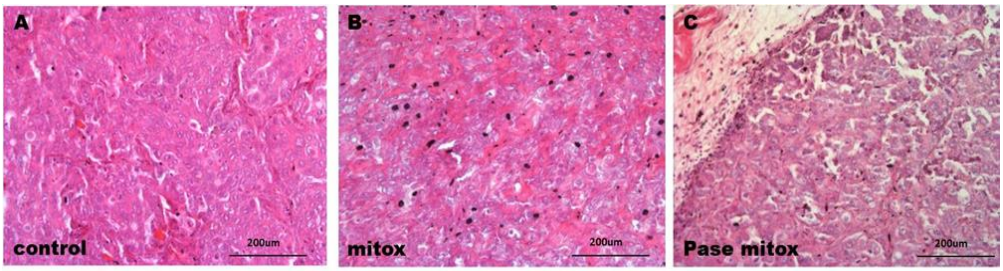

Figure 28. Histology of primary tumor mass. Images show the parenchyma of primary tumors in all the experimental groups. **A)** A representative image of primary tumor mass collected from the control group treated with saline; **B)** mice treated with free MIT; **C)** mice treated with HFt-MP-PASE-MIT.

4.2.7 Histological evaluation of other organs

Histological evaluation of lungs, kidneys, spleen, liver and heart specimens was performed for all the treated mice, in order to inspect any organ structural abnormalities and toxicity effects. Histology of different organ tissues, reported in **Figure 29**, showed that both MIT and HFt-MP-PASE-MIT did not exert any toxic effects on the overall architecture and organization of cells. The selected images portray representative profiles of other tissue sections; thus, reflecting the overall preserved structure of various organs unaffected by the type of applied drugs.

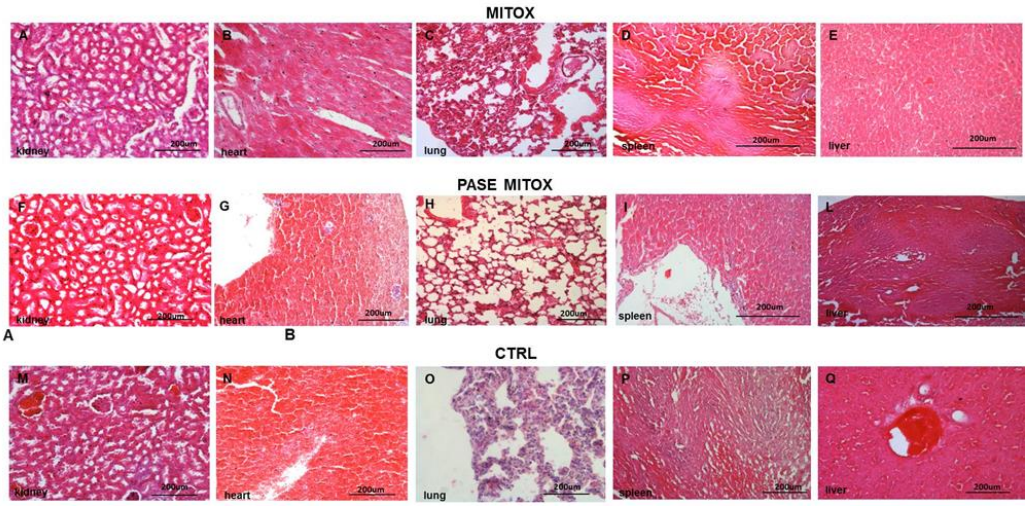

Figure 29. Histological evaluation of the integrity of the organ's architecture. Several tissues as kidneys, hearth, lungs, spleen and liver were explanted from mice at sacrifice. The panel shows light microscope images from mice treated with HFt-MP-PASE-MIT (images A,B,C,D,E), MIT (images F,G,H,I,L) or saline (images M,N,O,P,Q).

4.3 Design, Production and Characterization of The-05 variant of the HFt-MP-PASE nanocarrier

Our last aim in this PhD thesis was to modify the previously reported cancer-selective HFt-MP-PASE nanocarrier to enable it to efficiently encapsulate the potent anti-cancer drug Genz-644282. Due to the presence of basic moieties in this drug, we decided to enhance the negative charge of the internal cavity of the HFt component of the nanocarrier. Based on the analysis of the three-dimensional (3D) HFt structure, which was experimentally determined by X-ray crystallography and is available from the Protein Data Bank (PDB) (Lawson at al., 1991), we selected four native HFt residues, namely Lys53, Lys71, Thr135 and Lys143 to be mutated into negatively charged glutamic acid residues (**Figure 30**).

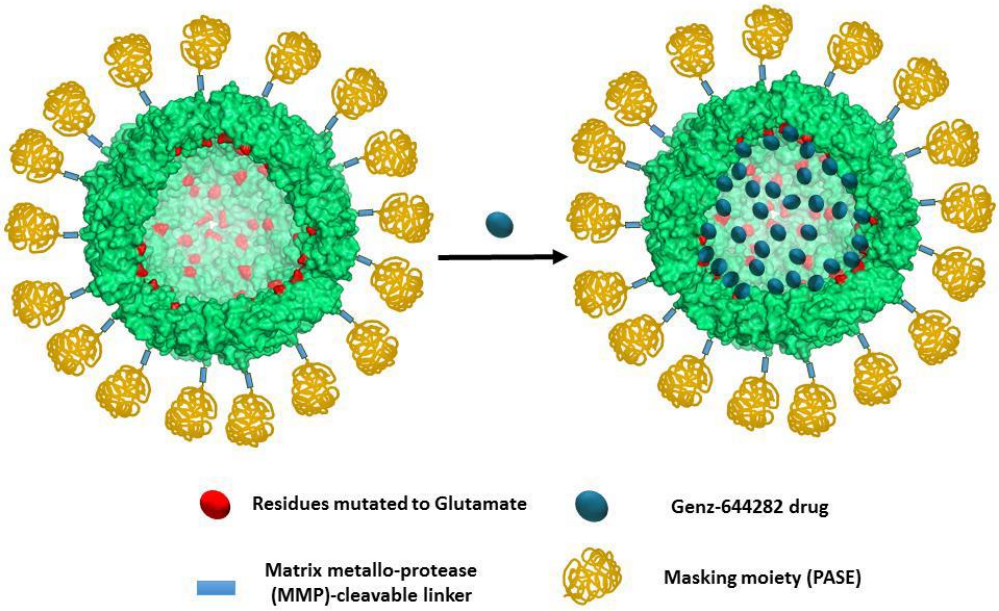

Figure 30. Schematic representation of The-0504 (The-05 incorporating Genz-644282 molecule) development. The Lys53, Lys71, Thr135 and Lys143 residues are mutated to Glutamate (Glu) in the The-05 protein (left), starting from the HFt-MP-PASE construct. Mutated residues are colored red. Metalloprotease cleavable sequence and PASE polypeptide are colored light blue and gold, respectively. Genz-644282 drug is colored blue. All other residues are light green. To allow the internal surface of the protein to be visualized (lighter colors), only 18 monomers out of 24 are shown. The picture has been generated with PyMol.

The resulting variant, named The-05, was obtained *via* recombinant protein technology and purified from the cellular soluble fraction at high yield (about 150 mg/L of *E. coli* cell culture at lab scale; about 3 g/L at 10 L high-density fermentation scale). The purity, size, and overall assembly of The-05 construct were analyzed by gel electrophoresis (SDS-PAGE), size-exclusion chromatography (SEC), dynamic light scattering (DLS) and transmission electron microscopy (TEM) experiments. In SDS-PAGE gel electrophoresis, The-05 migrated at about 35 kDa as single pure band (**Figure 31A**).

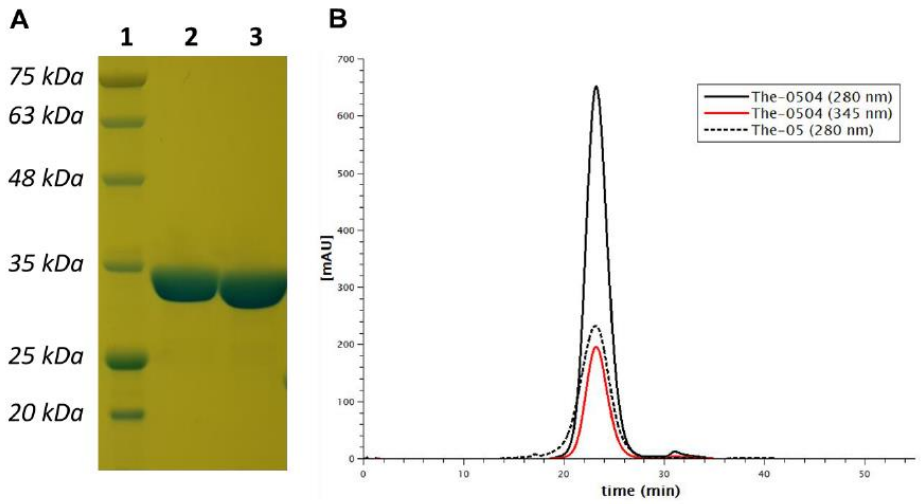

Figure 31. Purity of the The-05 nanocarrier before and after Genz-644282 encapsulation. (**A**) SDS-PAGE band migration profiles: Lane 1, protein marker; Lane 2, The-05 (10 µ g); Lane 3, The-0504 (10 µ g). (**B**) Size-exclusion chromatography analysis of The-05 and The-0504 detecting simultaneously The-05 protein and Genz-644282 contribution at 280nm (black) and 345nm (red), respectively.

Overall, samples were found to be highly pure and monodispersed in solution (**Figures 31B and 32A**). The mean diameter of The-05 was about 18.5 nm as assessed by DLS (17.8 ± 0.6 nm) and TEM (18.8 ± 1.7 nm) analyses (**Figure 32**). Moreover, microscopy images revealed that the protein retains the ability of native human ferritin to adopt a spherical structure (**Figure 32A**).

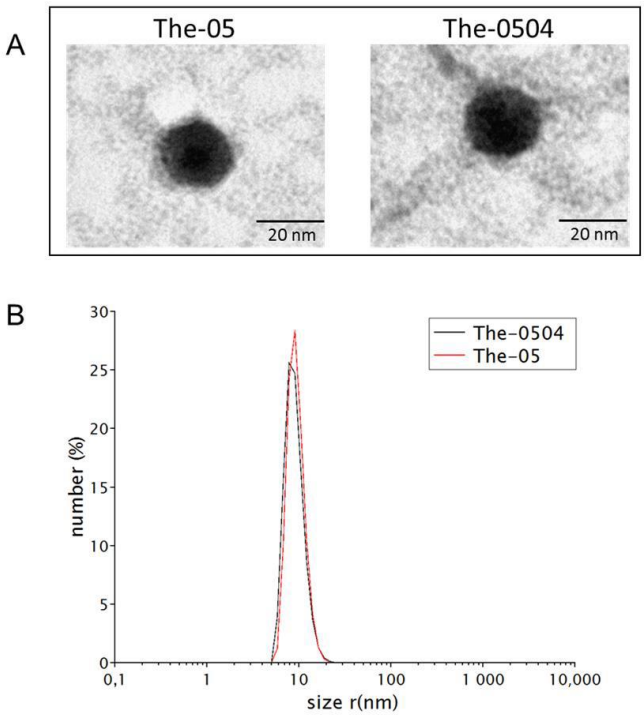

Figure 32. Biophysical characterization of the The-05 nanocarrier before and after Genz-644282 encapsulation. (**A**) Representative TEM images of negatively stained The-05 (left) and The-0504 (right), showing the spherical shape typical of ferritin-like proteins. (**B**) Dynamic light scattering profiles of The-05 (red) and The-0504 (black).

4.3.1 The-05 was loaded with Genz-644282 and the (The-0504) product was characterized

The non-camptothecin topoisomerase I inhibitor Genz-644282 was encapsulated inside the internal cavity of the novel The-05 construct by adapting the well-established protein disassembly/reassembly method (see **Scheme 1**). This procedure resulted in the encapsulation of about 80 molecules (81.0 ± 6.0) of the drug inside the The-05 cavity, with a protein recovery of

about 70%. The nanocarrier drug complex made by The-05 and the entrapped Genz-644282 was named The-0504 (**Figure 30**). By comparison, the original HFt-MP-PASE construct, which bears the native Lys53, Lys71, Thr135 and Lys143 residues on the internal surface, is significantly less effective since it encapsulates only about 15 (15.0 ± 2.1) Genz-644282 molecules, with a protein recovery of about 35%. To our knowledge, this is the first report describing the successful high-density encapsulation of the Genz-644282 drug in a nano-delivery system. Sample polydispersity and overall assembly were assessed by SEC, DLS and TEM experiments. No significant differences between samples were observed before (The-05) and after (The-0504) Genz-644282 encapsulation, indicating that this process does not affect the overall protein structure and assembly (**Figure 31**). The mean diameters of The-0504 were (17.0 ± 0.7 nm) and TEM (19.7 ± 1.5 nm) as assessed by DLS and TEM analyses, respectively. In addition, the chromatography elution pattern (SEC) shows co-elution of the protein (280 nm) and drug (345 nm) moieties, proving the composite nature of the produced material (**Figure 31B**). SEC profiling did not highlight any evidence hinting at compound aggregation or drug loss following The-0504 formulation as lyophilized powder, storage at 2–8 °C for four months, and reconstitution in water (data not shown). Longer storage times are currently under evaluation.

4.3.2 The-0504 shows high *in vitro* activity against different tumor cell lines

To assess the ability of Genz-644282-loaded The-0504 to kill cancer cells *in vitro*, we performed XTT viability assays on some human cancer cell

lines of gastrointestinal origin: colorectal (HT29) and pancreatic (PaCa44, HPAF II and MiaPaCa2) cancer cells. Results reported in **Figure 33** indicate that Genz-644282 encapsulated within The-05 nanocarrier maintains its pharmacological activity and has a cytotoxic activity comparable or even superior to that of free Genz-644282 in all tested cell lines. The relative compound concentration yielding 50% cell viability (IC50, nM) of The-0504 and free Genz-644282 are the following: 21.0 ± 2.1 (The-0504) and 160.3 ± 20.5 (Genz-644282) for HT-29 cells; 14.5 ± 1.6 (The-0504) and 26.1 ± 2.6 (Genz-644282) for MiaPaCa2 cells; 100.4 ± 19.3 (The-0504) and 150.4 ± 30.6 (Genz-644282) for PaCa44 cells; 35.9 ± 4.1 (The-0504) and 365.4 ± 58.0 (Genz-644282) for HPAF II cells. This is remarkable, since naked drugs can freely di use into cells, whereas The-0504 can only deliver the encapsulated Genz-644282 following rate-limiting receptor-mediated uptake. After these promising results, we decide to evaluate the preliminary antitumor activity of The-0504 *in vivo*.

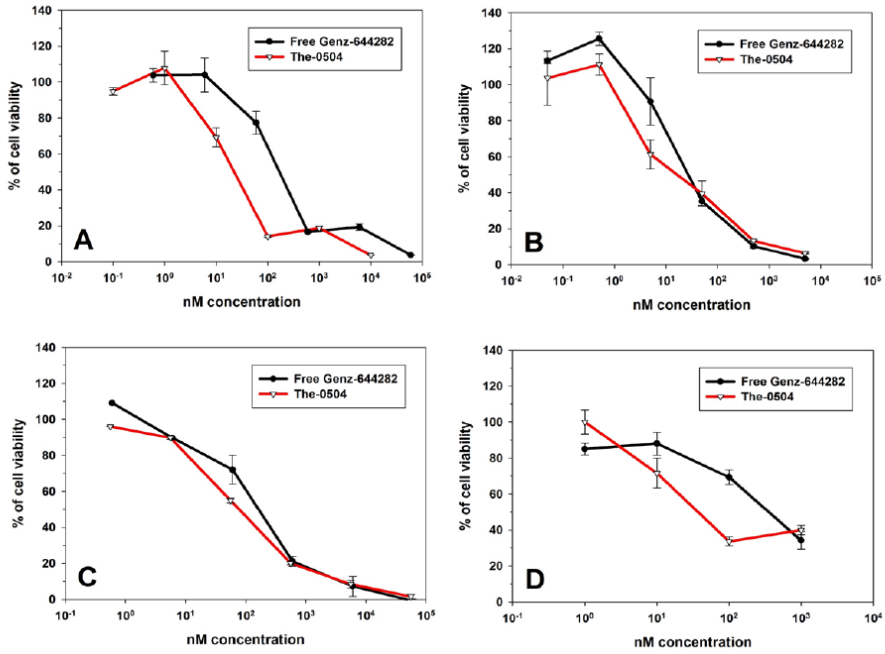

Figure 33. ***In vitro*** **cytotoxicity**. XTT assays performed on four cancer cell lines. (**A**) HT-29 colorectal cancer cells (**B**) MiaPaCa 2 pancreatic cancer cells; (**C**) PaCa44 pancreatic cancer cells and (**D**) HPAF II pancreatic cancer cells.

4.3.3 The-0504 is highly effective against a xenograft model of pancreatic cancer

Efficacy of The-0504 was evaluated in a xenograft (subcutaneous) model of pancreatic (HPAF II cells) cancer. Tumor-bearing animals were randomized when the tumor was about 80–100 mm³ and treated with free Genz-644282 and The-0504, both at 1.5 mg/kg in Genz-644282, twice a week for three consecutive weeks by intravenous injections. As shown in **Figure 34A**, HPAF II tumor growth was significantly inhibited in mice treated with 1.5 mg/kg free Genz-644282; conversely, in control groups, tumors grew

rapidly and reached a size >1,000 mm³ at days 20–25 after tumor cell injection. However, tumor growth stalled for a short period of time, and resumed as soon as treatment was discontinued reaching a size >1,000 mm³ at days 40. Tumor growth inhibition (TGI) value for free Genz-644282 was 53.3%. Strikingly, The-0504 showed a very high activity with a long-term regression of all established tumors. TGI value was 94.0%. Of note, 100% of mice treated with The-0504 were still alive at the end of the study period of 50 days from the beginning of therapy (**Figure 34B**), whereas the median survival of Genz-644282 treated-groups was 38.0 days. In addition, during the course of the experiment described above, mice were monitored for body weight and signs of pain or distress. No abnormal behavior or appreciable body-weight loss were observed in mice treated with The-0504.

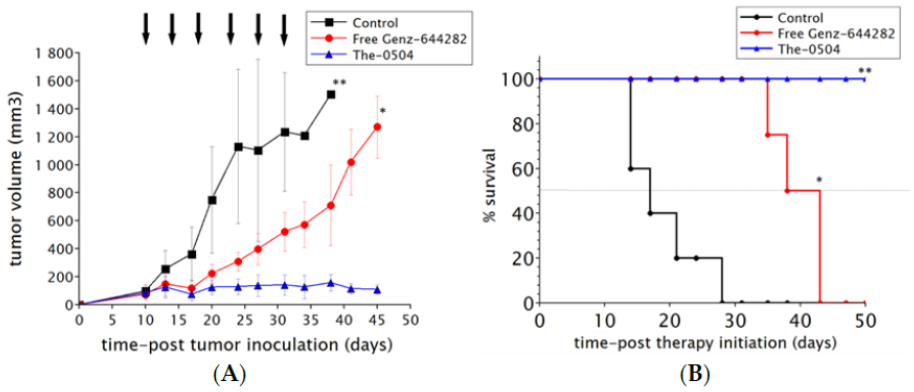

Figure 34. *In vivo* efficacy. (**A**) Tumor-growth curves for each mouse group are indicated-Student's t-test is used to determine statistical significance. Control vs The-0504 and Control vs Free Genz-644282: **p<0.005; Free Genz-644282 vs The-0504: * p 0.05. (**B**) Survival curves of different animal groups. Mice were sacrificed when the tumor had reached a volume in the range 1,000–1,500 mm³. Statistical analysis was performed by log-rank test. Control vs

The-0504, and Control vs Free Genz-644282: **p>0.005; Free Genz-644282 vs The-0504 mg/Kg: * p < 0.05.

5. CONCLUSIONS

5.1 Human HFt/CD71 complex

The identification of the residues involved in the complex between HFt and the CD71, an interaction widely exploited for nanotechnological applications of drug-delivery systems (de Turris et al., 2017; Fracasso et al., 2016; Zhen et al., 2013; Falvo et al., 2013) but so far unexplained in atomic details, was obtained during this PhD thesis, in collaboration with the group of Prof. Vallone (Sapienza University). The final cryo-EM map, obtained at 3.9 Å resolution (**Figure 14**), allowed to fit the atomic structures of the contact region without ambiguity: HFt and CD71 bind in a "virus-like" manner, i.e. HFt contacts the apical domain of CD71 (see **Figure 10** for comparison). Notably, this is the first time that HFt in complex with another protein has ever been imaged and resolved. The HFt binding region (**Figure 16** and **Figure 17**) is constituted by the external BC loop (R79, F81, Q83, K86, K87) and the N-terminus of both A and C helices (T5; Q14, D15, E17-A19, N21, R22, N25; E116, K119, D123). In conclusion, our work provides a sound structural basis to elaborate on the possibility of developing alternative ferritin-like anti-viral or anti-parasite therapeutic ligand, be it an antibody or a peptidomimetic capable of blocking the "common contacts" epitope on CD71 residue, and to further engineering ferritins as theranostic agents.

5.2 HFt-MP-PASE-MIT for cancer therapy

The results obtained along this PhD thesis work allowed also to present promising results from *in vitro* and *in vivo* applications of Mitoxantrone (MIT) drug loaded on HFt modified nanocages as effective means to control the growth of Pancreatic Cancer (PC) cells. Compared to freely unloaded MIT molecules, HFt-MP-PASE-MIT demonstrated a superimposable capability to kill and intoxicate tumor cells despite its large size and mode of entry using a receptor (CD71) mediated uptake process. Complementary data from *in vivo* experiments clearly demonstrated that when MIT is delivered to tumor mass by HFt nanocage, the growth of subcutaneous induced tumor is much slower, thereby prolonging the overall survival rate of treated mice (**Figure 25**). Our findings demonstrate an *in vivo* efficacy of our MIT variant that is superior to any other tested forms (Zhang et al., 2018). All this is achieved without compromising the overall health status of the mice and the structure of various body organs. Indeed, the histological analysis of various tissue organs clearly showed that both MIT and HFt-MP-PASE-MIT do not modify the architecture and cellular organization of the analyzed organs. In conclusion, HFt-MP-PASE-MIT offers a reliable and favourable nanoplatform that could be also effective in delivering various drugs to advance PC cancer therapy.

5.3 The-0504 for cancer therapy

The last aim of this PhD thesis was to design and develop a novel HFt-based construct that were superior in terms of efficacy for cancer therapy in comparison to previously developed ones. This novel HFt-based construct was named The-05 and was characterized by the following features with respect to the native HFt protein: (a) outer masking (PASE) shell; (b) tumor-selective

sequence responsive to proteolytic cleavage by MMPs; (c) 96 negatively charged glutamic acid residues inside the internal cavity for a better drug-binding and delivery (**Figure 30**). The-05 is expressed at high yields in *E. coli*; self-assembles into a wild-type like 24meric nanoparticle highly monodispersed; encapsulates stably up to 80 Genz-644282 molecules in the internal cavity. The-05 was named The-0504 after Genz-644282 encapsulation. Genz-644282 is a drug payload more potent and versatile than those previously used by our group. An *in vitro* assay demonstrated that The-0504 inhibited tumor cell proliferation with a slightly superior efficacy to the free drug Genz-644282 (**Figure 33**). Strikingly, The-0504 displayed excellent therapeutic efficacy in a human pancreatic cancer model *in vivo*, increasing animal overall survivals significantly. The *in vitro* and *in vivo* properties of Genz644282-loaded construct fully justify carrying out additional preclinical studies (in progress) to assess its real potential for cancer therapy.

6. REFERENCES

Abraham J, Corbett KD, Farzan M, Choe H, Harrison SC. *Structural basis for receptor recognition by New World hemorrhagic fever arenaviruses.* Nat Struct Mol Biol. 2010 Apr;17(4):438-44. doi: 10.1038/nsmb.1772. Epub 2010 Mar 7. PMID: 20208545; PMCID: PMC2920743.

Aggarwal BB, Vijayalekshmi RV, Sung B. *Targeting inflammatory pathways for prevention and therapy of cancer: short-term friend, long-term foe.* Clin Cancer Res. 2009 Jan 15;15(2):425-30. doi: 10.1158/1078-0432.CCR-08-0149. PMID: 19147746.

Alexis F, Pridgen EM, Langer R, Farokhzad OC. *Nanoparticle technologies for cancer therapy.* Handb Exp Pharmacol. 2010;(197):55-86.

Allen TM. *Ligand-targeted therapeutics in anticancer therapy*. Nat Rev Cancer. 2002 Oct;2(10):750-63. Review.

Arap W, Pasqualini R, Ruoslahti E. *Cancer treatment by targeted drug delivery to tumor vasculature in a mouse model. Science.* 1998 Jan 16;279(5349):377-80.

Aubin-Tam ME. *Conjugation of nanoparticles to proteins.* Methods Mol Biol. 2013;1025:19-27.

Baban DF, Seymour LW. *Control of tumour vascular permeability.* Adv Drug Deliv Rev. 1998 Oct 5;34(1):109-119.

Bao G, Mitragotri S, Tong S. *Multifunctional nanoparticles for drug delivery and molecular imaging.* Annu Rev Biomed Eng. 2013;15:253-82. Review.

Baronzio G, Schwartz L, Kiselevsky M, Guais A, Sanders E, Milanesi G, Baronzio M, Freitas I. *Tumor interstitial fluid as modulator of cancer inflammation, thrombosis, immunity and angiogenesis.* Anticancer Res. 2012 Feb;32(2):405-14.

Bedi D, Gillespie JW, Petrenko VA Jr, Ebner A, Leitner M, Hinterdorfer P, Petrenko VA. *Targeted delivery of siRNA into breast cancer cells via phage fusion proteins*. Mol Pharm. 2013 Feb 4;10(2):551-9.

Bellini M, Mazzucchelli S, Galbiati E, Sommaruga S, Fiandra L, Truffi M, Rizzuto MA, Colombo M, Tortora P, Corsi F, Prosperi D. *Protein nanocages for self-triggered nuclear delivery of DNA-targeted chemotherapeutics in Cancer Cells*. J Control Release. 2014 Dec 28;196:184-96.

Bennett MJ, Lebrón JA, Bjorkman PJ. *Crystal structure of the hereditary haemochromatosis protein HFE complexed with transferrin receptor*. Nature. 2000 Jan 6;403(6765):46-53. doi: 10.1038/47417. PMID: 10638746.

Birrer MJ, Moore KN, Betella I, Bates RC. Antibody-Drug Conjugate-Based *Therapeutics: State of the Science.* J Natl Cancer Inst. 2019 Jun 1;111(6):538-549. doi: 10.1093/jnci/djz035. PMID: 30859213.

Brown JM, Attardi LD. *The role of apoptosis in cancer development and treatment response.* Nat Rev Cancer. 2005 Mar;5(3):231-7. Review.

Calcabrini A, Meschini S, Stringaro A, Cianfriglia M, Arancia G, Molinari A. *Detection of P-glycoprotein in the nuclear envelope of multidrug resistant cells.* Histochem J. 2000 Oct;32(10):599-606.

Carter PJ, Lazar GA. *Next generation antibody drugs: pursuit of the 'high-hanging fruit'*. Nat Rev Drug Discov. 2018 Mar;17(3):197-223. doi: 10.1038/nrd.2017.227. Epub 2017 Dec 1. PMID: 29192287.

Ceci P, Morea V, Fornara M, Bellapadrona, G, Falvo E, and Ilari A. *Biomimetic materials synthesis by ferritin-related, cage-shaped proteins.* Adv. Topics in Biomineralization, 2012: Jong Seto (Ed.), ISBN: 978-953-51-0045-4, InTech.

Chen TT, Li L, Chung DH, Allen CD, Torti SV, Torti FM, Cyster JG, Chen CY, Brodsky FM, Niemi EC, Nakamura MC, Seaman WE, Daws MR. *TIM-2 is expressed on B cells and in liver and kidney and is a receptor for H-ferritin endocytosis.* J Exp Med. 2005 Oct 3;202(7):955-65. doi: 10.1084/jem.20042433. PMID: 16203866; PMCID: PMC2213179.

Cheng Y, Zak O, Aisen P, Harrison SC, Walz T. *Structure of the human transferrin receptor-transferrin complex*. Cell. 2004 Feb 20;116(4):565-76. doi: 10.1016/s0092-8674(04)00130-8. PMID: 14980223.

Cho K, Wang X, Nie S, Chen ZG, Shin DM. *Therapeutic nanoparticles for drug delivery in cancer.* Clin Cancer Res. 2008 Mar 1;14(5):1310-6. Review.

Corry DB, Kiss A, Song LZ, Song L, Xu J, Lee SH, Werb Z, Kheradmand F. *Overlapping and independent contributions of MMP2 and MMP9 to lung allergic inflammatory cell egression through decreased CC chemokines*. FASEB J. 2004 Jun;18(9):995-7.

Crichton RR, Boelaert JR. *Inorganic Biochemistry of Iron Metabolism from Molecular Mechanisms to Clinical Consequences*, 3rd Ed., *John Wiley and Sons, Chichester*, 2009 183–222.

Dalton AC, Barton WA. *Over-expression of secreted proteins from mammalian cell lines.* Protein Sci. 2014 May;23(5):517-25. doi: 10.1002/pro.2439. Epub 2014 Mar 11. PMID: 24510886; PMCID: PMC4005704.

Damiani V, Falvo E, Fracasso G, Federici L, Pitea M, De Laurenzi V, Sala G, Ceci P. *Therapeutic Efficacy of the Novel Stimuli-Sensitive Nano-Ferritins Containing Doxorubicin in a Head and Neck Cancer Model.* Int J Mol Sci. 2017 Jul 18;18(7):1555. doi: 10.3390/ijms18071555. PMID: 28718812; PMCID: PMC5536043.

Danhier F, Feron O, Préat V. *To exploit the tumor microenvironment: Passive and active tumor targeting of nanocarriers for anti-cancer drug delivery.* J Control Release. 2010 Dec 1;148(2):135-46.

Daniels TR, Bernabeu E, Rodríguez JA, Patel S, Kozman M, Chiappetta DA, Holler E, Ljubimova JY, Helguera G, Penichet ML. *The transferrin receptor and the targeted delivery of therapeutic agents against cancer.* Biochim Biophys Acta. 2012 Mar;1820(3):291-317.

de la Rica R, Matsui H. *Applications of peptide and protein-based materials in bionanotechnology.* Chem Soc Rev. 2010 Sep;39(9):3499-509. Review.

de Turris V, Cardoso Trabuco M, Peruzzi G, Boffi A, Testi C, Vallone B, Celeste Montemiglio L, Georges AD, Calisti L, Benni I, Bonamore A, Baiocco P. *Humanized archaeal ferritin as a tool for cell targeted*

delivery. Nanoscale. 2017 Jan 5;9(2):647-655. doi: 10.1039/c6nr07129e. PMID: 27942679.

Din FU, Aman W, Ullah I, Qureshi OS, Mustapha O, Shafique S, Zeb A. *Effective use of nanocarriers as drug delivery systems for the treatment of selected tumors.* Int J Nanomedicine. 2017 Oct 5;12:7291-7309. doi: 10.2147/IJN.S146315. PMID: 29042776; PMCID: PMC5634382.

Ding Y, Li S, Nie G. *Nanotechnological strategies for therapeutic targeting of tumor vasculature.* Nanomedicine (Lond). 2013 Jul;8(7):1209-22.

Domínguez-Vera JM, Fernández B, Gálvez N. *Native and synthetic ferritins for nanobiomedical applications: recent advances and new perspectives.* Future Med Chem. 2010 Apr;2(4):609-18. doi: 10.4155/fmc.09.171. PMID: 21426011.

Essa S, Rabanel JM, Hildgen P. *Characterization of rhodamine loaded PEG-g-PLA nanoparticles (NPs): effect of poly(ethylene glycol) grafting density.* Int J Pharm. 2011 Jun 15;411(1-2):178-87.

Falvo E, Malagrinò F, Arcovito A, Fazi F, Colotti G, Tremante E, Di Micco P, Braca A, Opri R, Giuffrè A, Fracasso G, Ceci P. *The presence of glutamate residues on the PAS sequence of the stimuli-sensitive nano-ferritin improves in vivo biodistribution and mitoxantrone encapsulation homogeneity*. J Control Release. 2018 Apr 10;275:177-185. doi: 10.1016/j.jconrel.2018.02.025. Epub 2018 Feb 20. PMID: 29474961.

Falvo E, Tremante E, Arcovito A, Papi M, Elad N, Boffi A, Morea V, Conti G, Toffoli G, Fracasso G, Giacomini P, Ceci P. *Improved Doxorubicin Encapsulation and Pharmacokinetics of Ferritin-Fusion Protein*

Nanocarriers Bearing Proline, Serine, and Alanine Elements. Biomacromolecules. 2016 Feb 8;17(2):514-22. doi: 10.1021/acs.biomac.5b01446. Epub 2015 Dec 30. PMID: 26686226.

Falvo E, Tremante E, Fraioli R, Leonetti C, Zamparelli C, Boffi A, Morea V, Ceci P, Giacomini P. *Antibody-drug conjugates: targeting melanoma with cisplatin encapsulated in protein-cage nanoparticles based on human ferritin.* Nanoscale. 2013 Dec 21;5(24):12278-85.

Fan K, Gao L, Yan X. *Human ferritin for tumor detection and therapy.* Wiley Interdiscip Rev Nanomed Nanobiotechnol. 2013 Jul-Aug;5(4):287-98.

Fan K, Cao C, Pan Y, Lu D, Yang D, Feng J, Song L, Liang M, Yan X. *Magnetoferritin nanoparticles for targeting and visualizing tumour tissues.* Nat Nanotechnol. 2012 Jun 17;7(7):459-64. Erratum in: Nat Nanotechnol. 2012 Dec;7(12):833.

Fares F, Ganem S, Hajouj T, Agai E. *Development of a long-acting erythropoietin by fusing the carboxyl-terminal peptide of human chorionic gonadotropin beta-subunit to the coding sequence of human erythropoietin.* Endocrinology. 2007 Oct;148(10):5081-7.

Ferrari R, Colombo C, Casali C, Lupi M, Ubezio P, Falcetta F, D'Incalci M, Morbidelli M, Moscatelli D. *Synthesis of surfactant free PCL-PEG brushed nanoparticles with tunable degradation kinetics.* Int J Pharm. 2013 Sep 10;453(2):551-9.

Fracasso G, Falvo E, Colotti G, Fazi F, Ingegnere T, Amalfitano A, Doglietto GB, Alfieri S, Boffi A, Morea V, Conti G, Tremante E, Giacomini P, Arcovito A, Ceci P. *Selective delivery of doxorubicin by novel stimuli-sensitive nano-ferritins overcomes tumor refractoriness.* J Control

Release. 2016 Oct 10;239:10-8. doi: 10.1016/j.jconrel.2016.08.010. Epub 2016 Aug 12. PMID: 27524282.

Friedman AD, Claypool SE, Liu R. *The smart targeting of nanoparticles. Curr Pharm Des.* 2013;19(35):6315-29. Review.

Galaup A, Gomez E, Souktani R, Durand M, Cazes A, Monnot C, Teillon J, Le Jan S, Bouleti C, Briois G, Philippe J, Pons S, Martin V, Assaly R, Bonnin P, Ratajczak P, Janin A, Thurston G, Valenzuela DM, Murphy AJ, Yancopoulos GD, Tissier R, Berdeaux A, Ghaleh B, Germain S. *Protection against myocardial infarction and no-reflow through preservation of vascular integrity by angiopoietin-like 4.* Circulation. 2012 Jan 3;125(1):140-9.

Gammella E, Buratti P, Cairo G, Recalcati S. *The transferrin receptor: the cellular iron gate.* Metallomics. 2017 Oct 18;9(10):1367-1375. doi: 10.1039/c7mt00143f. PMID: 28671201.

Gruszczyk J, Huang RK, Chan LJ, Menant S, Hong C, Murphy JM, Mok YF, Griffin MDW, Pearson RD, Wong W, Cowman AF, Yu Z, Tham WH. *Cryo-EM structure of an essential Plasmodium vivax invasion complex*. Nature. 2018 Jul;559(7712):135-139. doi: 10.1038/s41586-018-0249-1. Epub 2018 Jun 27. PMID: 29950717.

Gullotti E, Yeo Y. *Extracellularly activated nanocarriers: a new paradigm of tumor targeted drug delivery*. Mol Pharm. 2009 Jul-Aug;6(4):1041-51.

Harari D, Kuhn N, Abramovich R, Sasson K, Zozulya AL, Smith P, Schlapschy M, Aharoni R, Köster M, Eilam R, Skerra A, Schreiber G. *Enhanced in vivo efficacy of a type I interferon superagonist with*

extended plasma half-life in a mouse model of multiple sclerosis. J Biol Chem. 2014 Oct 17;289(42):29014-29.

Harrison PM, Arosio P. *The ferritins: molecular properties, iron storage function and cellular regulation.* Biochim Biophys Acta. 1996 Jul 31;1275(3):161-203. Review.

Heldin CH, Rubin K, Pietras K, Ostman A. *High interstitial fluid pressure - an obstacle in cancer therapy.* Nat Rev Cancer. 2004 Oct;4(10):806-13. Review.

Hnawate, Rm and P. Deore. *Nanoparticle - novel drug delivery system: A Review.* PharmaTutor; 2017. PRINT ISSN: 2394-6679 | E-ISSN: 2347-7881

Hobbs SK, Monsky WL, Yuan F, Roberts WG, Griffith L, Torchilin VP, Jain RK. *Regulation of transport pathways in tumor vessels: role of tumor type and microenvironment*. Proc Natl Acad Sci U S A. 1998 Apr 14;95(8):4607-12.

Howell M, Wang C, Mahmoud A, Hellermann G, Mohapatra SS, Mohapatra S. *Dual-function theranostic nanoparticles for drug delivery and medical imaging contrast: perspectives and challenges for use in lung diseases*. Drug Deliv Transl Res. 2013 Aug 1;3(4):352-63.

Huang K, Ma H, Liu J, Huo S, Kumar A, Wei T, Zhang X, Jin S, Gan Y, Wang PC, He S, Zhang X, Liang XJ. *Size-dependent localization and penetration of ultrasmall gold nanoparticles in cancer cells, multicellular spheroids, and tumors in vivo.* ACS Nano. 2012 May 22;6(5):4483-93.

Jain RK, Stylianopoulos T. *Delivering nanomedicine to solid tumors*. Nat Rev Clin Oncol. 2010 Nov;7(11):653-64. Review.

Jain RK. *Delivery of molecular and cellular medicine to solid tumors*. Adv Drug Deliv Rev. 2001 Mar 1;46(1-3):149-68. Review.

Jain RK. *Transport of molecules in the tumor interstitium: a review*. Cancer Res. 1987 Jun 15;47(12):3039-51. Review.

Jain RK. *Transport of molecules, particles, and cells in solid tumors*. Annu Rev Biomed Eng. 1999;1:241-63. Review.

Jang SH, Wientjes MG, Lu D, Au JL. *Drug delivery and transport to solid tumors.* Pharm Res. 2003 Sep;20(9):1337-50. Review.

Jones A, Harris AL. *New developments in angiogenesis: a major mechanism for tumor growth and target for therapy*. Cancer J Sci Am. 1998 Jul-Aug;4(4):209-17. Review.

Kanapathipillai M, Brock A, Ingber DE. *Nanoparticle targeting of anti-cancer drugs that alter intracellular signaling or influence the tumor microenvironment.* Adv Drug Deliv Rev. 2014 Dec 15;79-80:107-18.

Khoshnejad M, Parhiz H, Shuvaev VV, Dmochowski IJ, Muzykantov VR. *Ferritin-based drug delivery systems: Hybrid nanocarriers for vascular immunotargeting*. J Control Release. 2018 Jul 28;282:13-24. doi: 10.1016/j.jconrel.2018.02.042. Epub 2018 Mar 6. PMID: 29522833; PMCID: PMC6008199.

Köber C, Schmiedek F, Habermas T. *Characterizing lifespan development of three aspects of coherence in life narratives: a cohort-sequential study*.

Dev Psychol. 2015 Feb;51(2):260-75. doi: 10.1037/a0038668. PMID: 25621758.

Kotagiri N, Lee JS, Kim JW. *Selective pathogen targeting and macrophage evading carbon nanotubes through dextran sulfate coating and PEGylation for photothermal theranostics*. J Biomed Nanotechnol. 2013 Jun;9(6):1008-16.

Kreuter J. *Nanoparticles--a historical perspective.* Int J Pharm. 2007 Feb 22;331(1):1-10.

Krishna R, Mayer LD. *Multidrug resistance (MDR) in cancer. Mechanisms, reversal using modulators of MDR and the role of MDR modulators in influencing the pharmacokinetics of anticancer drugs*. Eur J Pharm Sci. 2000 Oct;11(4):265-83.

Kurtzberg LS, Roth S, Krumbholz R, Crawford J, Bormann C, Dunham S, Yao M, Rouleau C, Bagley RG, Yu XJ, Wang F, Schmid SM, Lavoie EJ, Teicher BA. *Genz-644282, a novel non-camptothecin topoisomerase I inhibitor for cancer treatment.* Clin Cancer Res. 2011 May 1;17(9):2777-87. doi: 10.1158/1078-0432.CCR-10-0542. Epub 2011 Mar 17. PMID: 21415217.

Kwon C, Kang YJ, Jeon S, Jung S, Hong SY, Kang S. *Development of protein-cage-based delivery nanoplatforms by polyvalently displaying β-cyclodextrins on the surface of ferritins through copper(I)-catalyzed azide/alkyne cycloaddition*. Macromol Biosci. 2012 Nov;12(11):1452-8.

Lammers T, Kiessling F, Hennink WE, Storm G. *Drug targeting to tumors: principles, pitfalls and (pre-) clinical progress.* J Control Release. 2012 Jul 20;161(2):175-87.

LaRocque J, Bharali DJ, Mousa SA. *Cancer detection and treatment: the role of nanomedicines. Mol Biotechnol.* 2009 Jul;42(3):358-66.

Lawrence CM, Ray S, Babyonyshev M, Galluser R, Borhani DW, Harrison SC. *Crystal structure of the ectodomain of human transferrin receptor.* Science. 1999 Oct 22;286(5440):779-82. doi: 10.1126/science.286.5440.779. PMID: 10531064

Leamon CP, Reddy JA. *Folate-targeted chemotherapy*. Adv Drug Deliv Rev. 2004 Apr 29;56(8):1127-41. Review.

Lebrón JA, Bennett MJ, Vaughn DE, Chirino AJ, Snow PM, Mintier GA, Feder JN, Bjorkman PJ. *Crystal structure of the hemochromatosis protein HFE and characterization of its interaction with transferrin receptor*. Cell. 1998 Apr 3;93(1):111-23. doi: 10.1016/s0092-8674(00)81151-4. PMID: 9546397.

Lee LA, Wang Q. *Adaptations of nanoscale viruses and other protein cages for medical applications.* Nanomedicine. 2006 Sep;2(3):137-49. Review.

Lei Y, Hamada Y, Li J, Cong L, Wang N, Li Y, Zheng W, Jiang X. *Targeted tumor delivery and controlled release of neuronal drugs with ferritin nanoparticles to regulate pancreatic cancer progression.* J Control Release. 2016 Jun 28;232:131-42. doi: 10.1016/j.jconrel.2016.03.023. Epub 2016 Apr 2. PMID: 27046157.

Li L, Fang CJ, Ryan JC, Niemi EC, Lebrón JA, Björkman PJ, Arase H, Torti FM, Torti SV, Nakamura MC, Seaman WE. *Binding and uptake of H-ferritin are mediated by human transferrin receptor-1*. Proc Natl Acad Sci U S A. 2010 Feb 23;107(8):3505-10.

Links M, Brown R. *Clinical relevance of the molecular mechanisms of resistance to anti-cancer drugs*. Expert Rev Mol Med 1999:1–21.

Lobatto ME, Fuster V, Fayad ZA, Mulder WJ. *Perspectives and opportunities for nanomedicine in the management of atherosclerosis.* Nat Rev Drug Discov. 2011 Oct 21;10(11):835-52. Review. Erratum in: Nat Rev Drug Discov. 2011 Dec;10(12):963.

Maeda H, Nakamura H, Fang J. *The EPR effect for macromolecular drug delivery to solid tumors: Improvement of tumor uptake, lowering of systemic toxicity, and distinct tumor imaging in vivo*. Adv Drug Deliv Rev. 2013 Jan;65(1):71-9.

Maeda H, Wu J, Sawa T, Matsumura Y, Hori K. *Tumor vascular permeability and the EPR effect in macromolecular therapeutics: a review.* J Control Release. 2000 Mar 1;65(1-2):271-84. Review.

Maeda H. *The enhanced permeability and retention (EPR) effect in tumor vasculature: the key role of tumor-selective macromolecular drug targeting.* Adv Enzyme Regul. 2001;41:189-207. Review.

Malam Y, Loizidou M, Seifalian AM. *Liposomes and nanoparticles: nanosized vehicles for drug delivery in cancer.* Trends Pharmacol Sci. 2009 Nov;30(11):592-9.

Martinez JO, Chiappini C, Ziemys A, Faust AM, Kojic M, Liu X, Ferrari M, Tasciotti E. *Engineering multi-stage nanovectors for controlled degradation and tunable release kinetics*. Biomaterials. 2013 Nov;34(33):8469-77.

Maruyama K, Ishida O, Takizawa T, Moribe K. *Possibility of active targeting to tumor tissues with liposomes.* Adv Drug Deliv Rev. 1999 Nov 10;40(1-2):89-102.

Matsumura Y, Maeda H. *A new concept for macromolecular therapeutics in cancer chemotherapy: mechanism of tumoritropic accumulation of proteins and the antitumor agent smancs*. Cancer Res. 1986 Dec;46(12 Pt 1):6387-92.

McDonald DM, Thurston G, Baluk P. *Endothelial gaps as sites for plasma leakage in inflammation.* Microcirculation. 1999 Mar;6(1):7-22. Review.

Moghimi SM, and Patel HM. *Serum-mediated recognition of liposomes by phagocytic cells of the reticuloendothelial system—the concept of tissue specificity.* Ad. Drug Delivery Rev. 1998. 32:45–60.

Nagy JA, Dvorak AM, Dvorak HF. *Vascular hyperpermeability, angiogenesis, and stroma generation.* Cold Spring Harb Perspect Med. 2012 Feb;2(2):a006544.

Nie S, Xing Y, Kim GJ, Simons JW. *Nanotechnology applications in cancer*. Annu Rev Biomed Eng. 2007;9:257-88. Review.

Okada H, Mak TW. *Pathways of apoptotic and non-apoptotic death in tumour cells*. Nat Rev Cancer. 2004 Aug;4(8):592-603. Review.

Overall CM, Kleifeld O. *Tumour microenvironment - opinion: validating matrix metalloproteinases as drug targets and anti-targets for cancer therapy.* Nat Rev Cancer. 2006 Mar;6(3):227-39. Review.

Paciotti GF, Myer L, Weinreich D, Goia D, Pavel N, McLaughlin RE, Tamarkin L. *Colloidal gold: a novel nanoparticle vector for tumor directed drug delivery.* Drug Deliv. 2004 May-Jun;11(3):169-83. doi: 10.1080/10717540490433895. PMID: 15204636.

Papisov MI. *Theoretical considerations of RES-avoiding liposomes: Molecular mechanics and chemistry of liposome interactions*. Adv Drug Deliv Rev. 1998 Jun 8;32(1-2):119-138.

Park J, Zhang Y, Vykhodtseva N, Jolesz FA, McDannold NJ. *The kinetics of blood brain barrier permeability and targeted doxorubicin delivery into brain induced by focused ultrasound.* J Control Release. 2012 Aug 20;162(1):134-42.

Peer D, Karp JM, Hong S, Farokhzad OC, Margalit R, Langer R. *Nanocarriers as an emerging platform for cancer therapy*. Nat Nanotechnol. 2007 Dec;2(12):751-60. Review.

Pérez-Herrero E, Fernández-Medarde A. *Advanced targeted therapies in cancer: Drug nanocarriers, the future of chemotherapy*. Eur J Pharm Biopharm. 2015 Jun;93:52-79. doi: 10.1016/j.ejpb.2015.03.018. Epub 2015 Mar 23. PMID: 25813885.

Perrault SD, Chan WC. *In vivo assembly of nanoparticle components to improve targeted cancer imaging*. Proc Natl Acad Sci U S A. 2010 Jun 22;107(25):11194-9.

Pettersen EF, Goddard TD, Huang CC, Couch GS, Greenblatt DM, Meng EC, Ferrin TE. *UCSF Chimera--a visualization system for exploratory research and analysis.* J Comput Chem. 2004 Oct;25(13):1605-12. doi: 10.1002/jcc.20084. PMID: 15264254.

Pozzi D, Colapicchioni V, Caracciolo G, Piovesana S, Capriotti AL, Palchetti S, De Grossi S, Riccioli A, Amenitsch H, Laganà A. *Effect of polyethyleneglycol (PEG) chain length on the bio-nano-interactions between PEGylated lipid nanoparticles and biological fluids: from nanostructure to uptake in cancer cells*. Nanoscale. 2014 Mar 7;6(5):2782-92. doi: 10.1039/c3nr05559k. Epub 2014 Jan 27. PMID: 24463404.

Radoshitzky SR, Kuhn JH, Spiropoulou CF, Albariño CG, Nguyen DP, Salazar-Bravo J, Dorfman T, Lee AS, Wang E, Ross SR, Choe H, Farzan M. *Receptor determinants of zoonotic transmission of New World hemorrhagic fever arenaviruses.* Proc Natl Acad Sci U S A. 2008 Feb 19;105(7):2664-9. doi: 10.1073/pnas.0709254105. Epub 2008 Feb 11. PMID: 18268337; PMCID: PMC2268193.

Robert X, Gouet P. *Deciphering key features in protein structures with the new ENDscript server*. Nucleic Acids Res. 2014 Jul;42(Web Server issue):W320-4. doi: 10.1093/nar/gku316. Epub 2014 Apr 21. PMID: 24753421; PMCID: PMC4086106.

Romberg B, Hennink WE, Storm G. *Sheddable coatings for long-circulating nanoparticles.* Pharm Res. 2008 Jan;25(1):55-71.

Rossin R, Pan D, Qi K, Turner JL, Sun X, Wooley KL, Welch MJ. *64Cu-labeled folate-conjugated shell cross-linked nanoparticles for tumor*

imaging and radiotherapy: synthesis, radiolabeling, and biologic evaluation. J Nucl Med. 2005 Jul;46(7):1210-8.

Roy PS, Saikia BJ. *Cancer and cure: A critical analysis*. Indian J Cancer. 2016 Jul-Sep;53(3):441-442. doi: 10.4103/0019-509X.200658. PMID: 28244479.

Rubin P, Casarett G. *Microcirculation of tumors. I. Anatomy, function, and necrosis*. Clin Radiol. 1966 Jul;17(3):220-9.

Sakamoto S, Kawabata H, Masuda T, Uchiyama T, Mizumoto C, Ohmori K, Koeffler HP, Kadowaki N, Takaori-Kondo A. *H-Ferritin Is Preferentially Incorporated by Human Erythroid Cells through Transferrin Receptor 1 in a Threshold-Dependent Manner*. PLoS One. 2015 Oct 6;10(10):e0139915. doi: 10.1371/journal.pone.0139915. PMID: 26441243; PMCID: PMC4595017.

Sakhrani NM, Padh H. *Organelle targeting: third level of drug targeting*. Drug Des Devel Ther. 2013 Jul 17;7:585-99.

Salmaso S. and Caliceti P. *Self Assembling Nano-composites for Protein Delivery: Supramolecular Interactions of Soluble Polymers with Protein Drugs.* International Journal of Pharmaceutics, 2013, 440, 111-123.

Sant S, Poulin S, Hildgen P. *Effect of polymer architecture on surface properties, plasma protein adsorption, and cellular interactions of pegylated nanoparticles.* J Biomed Mater Res A. 2008 Dec 15;87(4):885-95.

Singh S, DuPage A, Weaver AY, Sagert J, White C, Krimm M and Richardson J, "*Development of a probody drug conjugate (PDC) targeting CD71 for the treatment of solid tumors and lymphomas*" in AACR 107th Annual Meeting 2016, New Orleans, 2016.

Schlapschy M, Binder U, Börger C, Theobald I, Wachinger K, Kisling S, Haller D, Skerra A. *PASylation: a biological alternative to PEGylation for extending the plasma half-life of pharmaceutically active proteins*. Protein Eng Des Sel. 2013 Aug;26(8):489-501.

Shubik P. *Vascularization of tumors*. J Cancer Res Clin Oncol 1982;103:211–226. Review.

Sooryakumar D, Dexheimer TS, Teicher BA, Pommier Y. *Molecular and cellular pharmacology of the novel noncamptothecin topoisomerase I inhibitor Genz-644282*. Mol Cancer Ther. 2011 Aug;10(8):1490-9. doi: 10.1158/1535-7163.MCT-10-1043. Epub 2011 Jun 2. PMID: 21636699; PMCID: PMC3155218.

Steichen SD, Caldorera-Moore M, Peppas NA. *A review of current nanoparticle and targeting moieties for the delivery of cancer therapeutics.* Eur J Pharm Sci. 2013 Feb 14;48(3):416-27.

Sudimack J, Lee RJ. *Targeted drug delivery via the folate receptor*. Adv Drug Deliv Rev. 2000 Mar 30;41(2):147-62. Review.

Sun T, Zhang YS, Pang B, Hyun DC, Yang M, Xia Y. *Engineered nanoparticles for drug delivery in cancer therapy.* Angew Chem Int Ed Engl. 2014 Nov 10;53(46):12320-64.

Talekar M, Kendall J, Denny W, Garg S. *Targeting of nanoparticles in cancer: drug delivery and diagnostics.* Anticancer Drugs. 2011 Nov;22(10):949-62.

Thomas CR, Ferris DP, Lee JH, Choi E, Cho MH, Kim ES, Stoddart JF, Shin JS, Cheon J, Zink JI. *Noninvasive remote-controlled release of drug molecules in vitro using magnetic actuation of mechanized nanoparticles*. J Am Chem Soc. 2010 Aug 11;132(31):10623-5.

Todorich B, Zhang X, Slagle-Webb B, Seaman WE, Connor JR. *Tim-2 is the receptor for H-ferritin on oligodendrocytes.* J Neurochem. 2008 Dec;107(6):1495-505. doi: 10.1111/j.1471-4159.2008.05678.x. Epub 2008 Nov 5. PMID: 19014383.

Tortorella S, Karagiannis TC. *Transferrin receptor-mediated endocytosis: a useful target for cancer therapy*. J Membr Biol. 2014 Apr;247(4):291-307. doi: 10.1007/s00232-014-9637-0. Epub 2014 Feb 27. PMID: 24573305.

Truffi M, Fiandra L, Sorrentino L, Monieri M, Corsi F, Mazzucchelli S. Ferritin nanocages: *A biological platform for drug delivery, imaging and theranostics in cancer*. Pharmacol Res. 2016 May;107:57-65. doi: 10.1016/j.phrs.2016.03.002. Epub 2016 Mar 9. PMID: 26968122.

Vannucci L, Falvo E, Fornara M, Di Micco P, Benada O, Krizan J, Svoboda J, Hulikova-Capkova K, Morea V, Boffi A, Ceci P. *Selective targeting of melanoma by PEG-masked protein-based multifunctional nanoparticles.* Int J Nanomedicine. 2012;7:1489-509.

Vannucci L, Falvo E, Failla CM, Carbo M, Fornara M, Canese R, Cecchetti S, Rajsiglova L, Stakheev D, Krizan J, Boffi A, Carpinelli G, Morea V,

Ceci P. *In Vivo Targeting of Cutaneous Melanoma Using an Melanoma Stimulating Hormone-Engineered Human Protein Cage with Fluorophore and Magnetic Resonance Imaging Tracers*. J Biomed Nanotechnol. 2015 Jan;11(1):81-92.

Vannucci, L, Falvo, E, Ceci, P. *Multifunctional Protein-Based Nanoparticles for Cancer Theranosis*. 2014, A. Prokop et al. (eds.), Intracellular Delivery II, Fundamental Biomedical Technologies 7, DOI: 10.1007/978-94-017-8896-0_12.

Vasir JK, Labhasetwar V. *Targeted drug delivery in cancer therapy*. Technol Cancer Res Treat. 2005 Aug;4(4):363-74. Review.

Wang Z, Chui WK, Ho PC. *Nanoparticulate delivery system targeted to tumor neovasculature for combined anticancer and antiangiogenesis therapy*. Pharm Res. 2011 Mar;28(3):585-96.

Wu Y, Sefah K, Liu H, Wang R, Tan W. *DNA aptamer-micelle as an efficient detection/delivery vehicle toward cancer cells*. Proc Natl Acad Sci U S A. 2010 Jan 5;107(1):5-10.

Xiao K, Li Y, Luo J, Lee JS, Xiao W, Gonik AM, Agarwal RG, Lam KS. *The effect of surface charge on in vivo biodistribution of PEG-oligocholic acid based micellar nanoparticles.* Biomaterials. 2011 May;32(13):3435-46. doi: 10.1016/j.biomaterials.2011.01.021. Epub 2011 Feb 4. PMID: 21295849; PMCID: PMC3055170.

Xie J, Xu C, Kohler N, Hou Y, Sun S. *Controlled PEGylation of monodisperse Fe3O4 nanoparticles for reduced non-specific uptake by macrophage cells.* Adv Mater; 2007; 19(20):3163.

Yu MK, Park J, Jon S. *Targeting strategies for multifunctional nanoparticles in cancer imaging and therapy*. Theranostics. 2012;2(1):3-44.

Zhang, L. et al. *H-Chain ferritin: a natural nuclei targeting and bioactive delivery nanovector*. Adv. Healthc. Mater. 4, 1305–1310 (2015).

Zhen Z, Tang W, Chen H, Lin X, Todd T, Wang G, Cowger T, Chen X, Xie J. *RGD-modified apoferritin nanoparticles for efficient drug delivery to tumors.* ACS Nano. 2013 Jun 25;7(6):4830-7.

7. APPENDIX

Publications produced during this Ph.D thesis:

Attachment I: Conti G,* **Pitea M**,* Ossanna R, Opri R, Tisci G, Falvo E, Innamorati G, Ghanem E, Sbarbati A, Ceci P, Fracasso G. *Mitoxantrone-loaded nanoferritin slows tumor growth and improves the overall survival rate in a subcutaneous pancreatic cancer mouse model.* Biomedicines. 2021 (***Submitted*****)**

Attachment II: Falvo E, Arcovito A, Conti G, Cipolla G, **Pitea M**, Morea V, Damiani V, Sala G, Fracasso G, Ceci P. *Engineered Human Nanoferritin Bearing the Drug Genz-644282 for Cancer Therapy*. Pharmaceutics. 2020 Oct 20;12(10):992. doi: 10.3390/pharmaceutics12100992. PMID: 33092088; PMCID: PMC7589674.

Attachment III: Montemiglio LC, Testi C, Ceci P, Falvo E, **Pitea M**, Savino C, Arcovito A, Peruzzi G, Baiocco P, Mancia F, Boffi A, des Georges A, Vallone B. *Cryo-EM structure of the human ferritin-transferrin receptor 1 complex*. Nat Commun. 2019 Mar 8;10(1):1121. doi: 10.1038/s41467-019-09098-w. PMID: 30850661; PMCID: PMC6408514.

*These two authors are contributed equally to the work

biomedicines

MDPI

Article

Mitoxantrone-loaded nanoferritin slows tumor growth and improves the overall survival rate in a subcutaneous pancreatic cancer mouse model

Giamaica Conti[1§], Martina Pitea[2,3§], Riccardo Ossanna[1], Roberta Opri[4], Giada Tisci[2], Elisabetta Falvo[5], Giulio Innamorati[6], Esther Ghanem[7], Andrea Sbarbati[1#], Pierpaolo Ceci[5*#] and Giulio Fracasso[4*#]

[1] Department of Neurological and Movement Sciences, University of Verona, 37134 Verona, Italy; giamaica.conti@univr.it (G.C.); riccardo.ossanna@univr.it (R.O.); andrea.sbarbati@univr.it (A.S.);
[2] Department of Biochemical Sciences, University Sapienza, 00185 Rome, Italy; martina.pitea@uniroma1.it (M.P.); tisci.1887341@studenti.uniroma1.it (G.T.)
[3] Center for Life Nano Science @ Sapienza, Istituto Italiano di Tecnologia, Rome 00161, Italy
[4] Department of Medicine, University of Verona, 37134 Verona, Italy; roberta.opri@gmail.com (RO.OP.); giuli.fracasso@univr.it (G.F.)
[5] CNR–National Research Council of Italy, Institute of Molecular Biology and Pathology, 00185 Rome, Italy; elisabetta.falvo@cnr.it (E.F.); Pierpaolo.ceci@cnr.it (P.C.)
[6] Department of Surgical Sciences, Dentistry, Gynecology and Pediatrics, Section of Surgery, University of Verona, 37134 Verona, Italy; giulio.innamorati@univr.it (G.I.)
[7] Department of Sciences, Notre Dame University - Louaize, Zouk Mosbeh, Lebanon; eghanem@ndu.edu.lb (E.G.)

* Correspondence: giulio.fracasso@univr.it (G.F.); pierpaolo.ceci@cnr.it (P.C.); Tel.: +39-0458126449 (G.F.); +39-0649910761 (P.C.)

§ These authors contributed equally to this work
# Share Senior Authorship

Citation: Lastname, F.; Lastname, F. Lastname, F. Title. *Biomedicines* 2021, 9, x. https://doi.org/10.3390/xxxxx

Academic Editor: Firstname Last-

Abstract: Pancreatic cancer (PC) represents an intriguing topic for researchers. To date, the prognosis of metastized PC is poor with just 7% of patients exceeding a five-year survival period. Thus, molecular modifications of existing drugs should be developed to change the course of the disease. Our previously generated nanocages of Mitoxantrone (MIT) encapsulated in human H-chain Ferritin (HFt), designated as HFt-MP-PASE-MIT, has shown excellent tumor distribution and extended serum half-life meriting further investigation for PC treatment. Thus in this study, we used the same nano-formulation to test its cytotoxicity using both *in vitro* and *in vivo* assays. Interestingly, both encapsulated and free-MIT drugs demonstrated similar killing capabilities on PaCa44 cell line. Conversely, *in vivo* assessment in a subcutaneous PaCa44 tumor model of PC demonstrated a remarkable capability for encapsulated MIT to control tumor growth and improve mouse survival with a median survival rate of 65 *vs* 33 days for loaded and free-MIT, respectively. Interestingly, throughout the course of mice treatment, MIT encapsulation did not present any adverse side effects as confirmed by histological analysis of various murine tissue organs and body mass weights. Our results are promising and pave the way to effective PC targeted chemotherapy using our HFt nanodelivery platforms.

pharmaceutics

MDPI

Article

Engineered Human Nanoferritin Bearing the Drug Genz-644282 for Cancer Therapy

Elisabetta Falvo [1,†], Alessandro Arcovito [2,3,†], Giamaica Conti [4], Giuseppe Cipolla [5], Martina Pitea [6], Veronica Morea [1], Verena Damiani [7], Gianluca Sala [7], Giulio Fracasso [8,*,‡] and Pierpaolo Ceci [1,5,*,‡]

1 CNR–National Research Council of Italy, Institute of Molecular Biology and Pathology, 00185 Rome, Italy; elisabetta.falvo@cnr.it (E.F.); veronica.morea@cnr.it (V.M.)
2 Dipartimento di Scienze Biotecnologiche di Base, Cliniche Intensivologiche e Perioperatorie, Università Cattolica del Sacro Cuore, Largo F. Vito 1, 00168 Rome, Italy; alessandro.arcovito@Unicatt.it
3 Fondazione Policlinico Agostino Gemelli, IRCCS, 00168 Rome, Italy
4 Department of Neurological and Movement Sciences, University of Verona, 37134 Verona, Italy; giamaica.conti@univr.it
5 Thena Biotech, 04100 Latina, Italy; giuseppecipolla92@gmail.com
6 Department of Biochemical Sciences, University Sapienza, 00185 Rome, Italy; martina.pitea@uniroma1.it
7 Center for Advanced Studies and Technology (CAST), Department of Medical Oral and Biotechnological Sciences, University of Chieti-Pescara, 66100 Chieti, Italy; verena.damiani@unich.it (V.D.); g.sala@unich.it (G.S.)
8 Department of Medicine, University of Verona, 37134 Verona, Italy
* Correspondence: giulio.fracasso@univr.it (G.F.); pierpaolo.ceci@cnr.it (P.C.); Tel.: +39-0458126449 (G.F.); +39-0649910761 (P.C.)
† These authors contributed equally to this work.
‡ Co-senior authors.

Received: 1 October 2020; Accepted: 16 October 2020; Published: 20 October 2020

Abstract: Gastrointestinal tumors, including pancreatic and colorectal cancers, represent one of the greatest public health issues worldwide, leading to a million global deaths. Recent research demonstrated that the human heavy chain ferritin (HFt) can encapsulate different types of drugs in its cavity and can bind to its receptor, CD71, in several solid and hematological tumors, thus highlighting the potential use of ferritin for tumor-targeting therapies. Here, we describe the development and characterization of a novel nanomedicine based on the HFt that is named The-0504. In particular, this novel system is a nano-assembly comprising an engineered version of HFt that entraps about 80 molecules of a potent, wide-spectrum, non-camptothecin topoisomerase I inhibitor (Genz-644282). The-0504 can be produced by a standardized pre-industrial process as a pure and homogeneously formulated product with favourable lyophilization properties. The preliminary anticancer activity was evaluated in cultured cancer cells and in a mouse model of pancreatic cancer. Overall results reported here make The-0504 a candidate for further preclinical development against CD-71 expressing deadly tumors.

Keywords: nanomedicine; human ferritin; gastrointestinal tumors; non-camptothecin topoisomerase I inhibitors; drug-delivery; CD71

1. Introduction

Protein-cage molecules based on the H-chain of human ferritin (HFt) have been recently attracting growing interest in the field of cancer drug delivery, due to their excellent biocompatibility, selectivity for cancer over normal cells, binding to a large number of different human tumors and ability to

nature COMMUNICATIONS

ARTICLE

https://doi.org/10.1038/s41467-019-09098-w OPEN

Cryo-EM structure of the human ferritin–transferrin receptor 1 complex

Linda Celeste Montemiglio[1,2,3], Claudia Testi[1,4], Pierpaolo Ceci[2], Elisabetta Falvo[2], Martina Pitea[1], Carmelinda Savino[2], Alessandro Arcovito[5,6], Giovanna Peruzzi[4], Paola Baiocco[4], Filippo Mancia[7], Alberto Boffi[1], Amédée des Georges[8,9,10] & Beatrice Vallone[1,3]

Human transferrin receptor 1 (CD71) guarantees iron supply by endocytosis upon binding of iron-loaded transferrin and ferritin. Arenaviruses and the malaria parasite exploit CD71 for cell invasion and epitopes on CD71 for interaction with transferrin and pathogenic hosts were identified. Here, we provide the molecular basis of the CD71 ectodomain-human ferritin interaction by determining the 3.9 Å resolution single-particle cryo-electron microscopy structure of their complex and by validating our structural findings in a cellular context. The contact surfaces between the heavy-chain ferritin and CD71 largely overlap with arenaviruses and *Plasmodium vivax* binding regions in the apical part of the receptor ectodomain. Our data account for transferrin-independent binding of ferritin to CD71 and suggest that select pathogens may have adapted to enter cells by mimicking the ferritin access gate.

[1] Department of Biochemical Sciences "Alessandro Rossi Fanelli", Sapienza University of Rome, P.le A. Moro 5, 00185 Rome, Italy. [2] Institute of Molecular Biology and Pathology, National Research Council, P.le A. Moro 5, 00185 Rome, Italy. [3] Istituto Pasteur-Fondazione Cenci Bolognetti, Dipartimento di Scienze Biochimiche "A. Rossi Fanelli", Sapienza Università di Roma, P.le A. Moro 5, 00185 Rome, Italy. [4] Center for Life Nano Science @ Sapienza, Istituto Italiano di Tecnologia, V.le Regina Elena 291, 00161 Rome, Italy. [5] Istituto di Biochimica e Biochimica Clinica, Università Cattolica del Sacro Cuore, Largo F. Vito 1, 00168 Rome, Italy. [6] Fondazione Policlinico Universitario Agostino Gemelli-IRCCS, Largo F. Vito 1, 00168 Rome, Italy. [7] Department of Physiology and Cellular Biophysics, Russ Berrie Pavilion, Columbia University Medical Center, 1150 St Nicholas Ave, New York, NY 10032, USA. [8] Advanced Science Research Center at The Graduate Center of the City University of New York, 85 Saint Nicholas Terrace, New York, NY 10031, USA. [9] Department of Chemistry and Biochemistry, City College of New York, New York, NY 10031, USA. [10] Programs in Biochemistry and Chemistry, The Graduate Center of the City University of New York, New York, NY 10016, USA. These authors contributed equally: Linda Celeste Montemiglio, Claudia Testi. Correspondence and requests for materials should be addressed to A.d.G. (email: amedee.desgeorges@lasrc.cuny.edu) or to B.V. (email: beatrice.vallone@uniroma1.it)